Monthly Notices
of the
ROYAL ASTRONOMICAL SOCIETY

Mon. Not. R. Astron. Soc. **422,** 3189–3207 (2012) doi:10.1111/j.1365-2966.2012.20841.x

Semi-analytic modelling of the extragalactic background light and consequences for extragalactic gamma-ray spectra

Rudy C. Gilmore,[1,2]★ Rachel S. Somerville,[3,4] Joel R. Primack[2] and Alberto Domínguez[5,6,7,8]†

[1]*SISSA, via Bonomea 265, 34136 Trieste, Italy*
[2]*University of California, Santa Cruz, CA 95064, USA*
[3]*Space Telescope Science Institute, Baltimore, MD 21218, USA*
[4]*Department of Physics and Astronomy, The Johns Hopkins University, Baltimore, MD 21218, USA*
[5]*Santa Cruz Institute for Particle Physics (SCIPP), University of California, Santa Cruz, CA 95064, USA*
[6]*Instituto de Astrofísica de Andalucía, CSIC, Apdo. Correos 3004, E-18080 Granada, Spain*
[7]*Departamento de Física Atómica, Molecular y Nuclear, Universidad de Sevilla, Apdo. Correos 1065, E-41080 Sevilla, Spain*
[8]*Department of Physics and Astronomy, University of California, Riverside, CA 92521, USA*

Accepted 2012 February 28. Received 2012 January 31; in original form 2011 April 4

ABSTRACT

Attenuation of high-energy gamma-rays by pair production with ultraviolet, optical and infrared (IR) extragalactic background light (EBL) photons provides a link between the history of galaxy formation and high-energy astrophysics. We present results from our latest semi-analytic models (SAMs), which employ the main ingredients thought to be important to galaxy formation and evolution, as well as an improved model for reprocessing of starlight by dust to mid- and far-IR wavelengths. These SAMs are based upon a Λ cold dark matter hierarchical structural formation scenario, and are successful in reproducing a large variety of observational constraints such as number counts, luminosity and mass functions and colour bimodality. Our fiducial model is based upon a *Wilkinson Microwave Anisotropy Probe* 5-year cosmology, and treats dust emission using empirical templates. This model predicts a background flux considerably lower than optical and near-IR measurements that rely on subtraction of zodiacal and galactic foregrounds, and near the lower bounds set by number counts of resolvable sources at a large number of wavelengths. We also show the results of varying cosmological parameters and dust attenuation model used in our SAM. For each EBL prediction, we show how the optical depth due to electron–positron pair production is affected by redshift and gamma-ray energy, and the effect of gamma-ray absorption on the spectra of a variety of extragalactic sources. We conclude with a discussion of the implications of our work, comparisons to other models and key measurements of the EBL and a discussion of how the burgeoning science of gamma-ray astronomy will continue to help constrain cosmology. The low EBL flux predicted by our fiducial model suggests an optimistic future for further studies of distant gamma-ray sources.

Key words: cosmology: theory – diffuse radiation – gamma-rays: general – infrared: diffuse background.

1 INTRODUCTION

The extragalactic background light (EBL) is the totality of light emitted by stars and active galactic nuclei (AGN) over the lifetime of the Universe. Today, this pervasive photon background consists of light emitted at all epochs, modified by redshifting and dilution due to the expansion of the universe. The bulk of the EBL occurs at wavelengths from the near-ultraviolet (UV) to the far-infrared (IR). In the UV, optical and near-IR most of the EBL is due to direct starlight, as well as a subdominant contribution from AGN (Schirber & Bullock 2003). From the mid-IR to submillimetre wavelengths, the EBL consists of reemitted light from dust particles, including both continuum thermal radiation and line emission from polycyclic aromatic hydrocarbons (PAH) molecules (Lagache, Puget & Dole 2005). The background at longer wavelengths is dominated by the cosmic microwave background, while shortward of the Lyman limit

★E-mail: rgilmore@sissa.it
†Visiting researcher at the Santa Cruz Institute for Particle Physics (SCIPP).

the background flux decreases rapidly due to attenuation by neutral hydrogen in stellar atmospheres and the interstellar and intergalactic media.

Because the production of the EBL is directly linked to the star formation history of the universe, limits on the EBL can be used to provide constraints on the history of galaxy formation and evolution. Observations of the extragalactic sky brightness can constrain the local background, however, they do not provide information about evolution of the background with redshift. Direct sky photometry has been attempted with a number of instruments, most notably Diffuse Infrared Background Experiment (DIRBE) and Far-Infrared Absolute Spectrophotometer (FIRAS), and also ground-based optical telescopes (e.g. Mattila et al. 2011), but these type of measurements are subject to considerable uncertainties due to the large foreground sources that must be subtracted (Hauser & Dwek 2001). Integration over discrete sources seen in galaxy surveys (e.g. Madau & Pozzetti 2000; Keenan et al. 2010) is another way to estimate the EBL, but one that in principle can only provide a lower limit due to the possibility of unseen sources beyond the magnitude limits of the survey instrument or underestimation of true total luminosity of galaxies due to light in the faint outskirts (e.g. Bernstein 2007). Observations with highly sensitive satellite instruments have provided us with EBL lower limits from galaxy number counts across wide wavelength ranges.

High-energy gamma-rays can interact with EBL photons in electron–positron pair production interactions (Nikishov 1962; Jelley 1966; Gould & Schreder 1967). By effectively removing these gamma-rays from view, this process has the potential to alter the observed spectra of extragalactic high-energy sources, and increasingly occlude those at higher redshifts. The rapid development of ground-based gamma-ray astronomy in the past 20 yr has led to a number of attempts – e.g. Dwek & Krennrich (2005), Aharonian et al. (2006), Mazin & Raue (2007), Albert et al. (2008) – to constrain the EBL based on modification to gamma-ray spectra, a method that can provide a measurement of the EBL that is independent of direct observation. In principle, the cosmological history of the EBL could be reconstructed by comparing observations of high-energy sources at different redshifts to their intrinsic spectra. Unfortunately, the emission mechanisms and intrinsic spectra of GeV and TeV sources are still poorly understood.

Understanding how the EBL is produced and how its spectral energy distribution (SED) evolves in redshift requires an understanding of the sources responsible for its production. This has been attempted by different authors using a variety of techniques. As enumerated in Domínguez et al. (2011, hereafter D11), calculations of the EBL fall into four general categories: (i) forward evolution beginning with initial cosmological conditions, such as the semi-analytic models (SAMs) used in this work; (ii) backwards evolution of the well-constrained present-day galaxy emissivity according to some prescription; (iii) evolution of galaxy properties that are inferred over some range in wavelength; (iv) direct observation of evolution in galaxy properties over the redshifts providing the major contribution to the background light, a category which describes the empirical method developed in D11.

The last two of these have become much more powerful techniques in recent years due to large-scale surveys by ground- and space-based instruments, especially at UV and IR wavelengths, where a great deal of progress has taken place in the last decade. Some of the first models to account for EBL production by the evolving galaxy population were Madau, Pozzetti & Dickinson (1998) and Franceschini (2001), using *Hubble Space Telescope* (*HST*) and *Infrared Space Observatory* (*ISO*) data, respectively, and Pei, Fall & Hauser (1999), who looked at chemical enrichment data in Lyα systems. A two-part paper series by Kneiske and collaborators (Kneiske, Mannheim & Hartmann 2002; Kneiske et al. 2004) computed the EBL and subsequently predictions for attenuation of gamma-ray sources based on a parametrization of the star formation rate (SFR) density. These models separately include the contribution of the luminous infrared galaxy (LIRG)/ultraluminous infrared galaxy (ULIRG) population. An update to this work by Kneiske & Dole (2010) attempt to create a model using a similar method that produces a minimal background, and a similar method was employed in Razzaque, Dermer & Finke (2009) and Finke, Razzaque & Dermer (2010). The aforementioned work of D11 used observed evolution up to $z = 4$ in the K-band luminosity function combined with the evolving distribution of 25 galaxy SED types from a multiwavelength survey of galaxies to estimate the EBL and its evolution.

Other authors have used backward evolution models to predict the EBL. These calculations begin with the present day galaxy luminosity function and attempt to trace this function backwards in time by assuming a functional form for the redshift evolution. In Malkan & Stecker (1998, 2001), IR luminosity functions from *IRAS* were extrapolated backwards in redshift using power-law functions. The model of Stecker, Malkan & Scully (2006) updated this work and computed the EBL below the Lyman limit (13.6 eV) for two different cases of stellar evolution. The model of Rowan-Robinson (2001) also utilized a 60 μm evolving luminosity function, and a four-component spectral model for IR and optical emission. One potential problem with this method is that it has difficulty accounting for the emissivity contribution of merger-triggered starbursts, believed to contribute an increasing fraction of the SFR density and IR emissivity with increasing redshift. Franceschini et al. (2001) made an attempt to account for this starburst phase in a backwards evolution model. Franceschini, Rodighiero & Vaccari (2008) published a sophisticated model using observed luminosity functions, and used it to calculate the EBL and gamma-ray attenuation. This model uses evolving luminosity functions in the near-IR up to $z = 1.4$ for two different galaxy populations (spiral and spheroidal) and local luminosity functions for the irregular/starbursting population, combined with synthetic SEDs to find the total emissivity.

In forward evolution scenarios such as SAMs, predictions for the evolution of galaxy emissivities are made by beginning from the universe in its primordial state and simulating the process of galaxy formation. This is considerably more involved and challenging than the other methods of estimating the EBL, but can provide a degree of insight into the fundamental astrophysics processes that determine the emissivity that is lacking in other approaches. SAMs of structure formation based on cold dark matter (CDM) merger trees have been used in several papers by our group to predict the EBL. Primack et al. (1999) predicted the EBL using the SAM described in Somerville & Primack (1999) and Somerville, Primack & Faber (2001). Later work included improved treatment of absorption and reemission of starlight by dust and updated cosmological data (Primack, Bullock & Somerville 2005; Primack, Gilmore & Somerville 2008).

In a companion paper to this work, Somerville et al. (2012, hereafter SGPD12), we present a new SAM based on galaxy formation in a *Wilkinson Microwave Anisotropy Probe* 5-year (*WMAP*5) cosmology. This model, which will be summarized in the next section, incorporates the physical processes thought to be most important in determining the evolution of these systems. From the luminosity density calculated in this model, we have predicted the evolving EBL out to high redshift. In this paper, we address the topic of gamma-ray attenuation and show how our estimated EBL affects

high-energy observations of extragalactic sources, and discuss the ability of gamma-ray telescopes to explore the distant universe. We also present a comprehensive comparison to the predictions for EBL and gamma-ray opacity that have been proposed by a number of recent authors. Our current work is an update to Primack et al. (2008), which presents an earlier stage of our results using a 'concordance cosmology' (CΛCDM), with parameters largely consistent with *WMAP*1. This work is also closely related and complementary to Gilmore et al. (2009), which used the CΛCDM model as the basis for a prediction of the UV background radiation out to high redshift, and therefore emphasized the calculation of optical depths for gamma-rays below 200 GeV. In that paper we included contributions to the UV emissivity from quasars, as well as an account of the attenuation of ionizing radiation escaping from galaxies and processing by neutral hydrogen in the intergalactic medium (IGM) using a radiative transfer code.

In the following section, we briefly review the key elements of the SAM presented in SGPD12. Results are presented in Section 3, beginning with a review of key results related to the evolving background radiation from SGPD12 in Subsection 3.1. In Subsection 3.2, we show how the population of photons in our calculated EBL impacts observations of extragalactic gamma-ray sources through pair production interactions. Subsection 3.3 deals with the comparison between our predicted gamma-ray optical depths and observations of very high energy (VHE) blazars, and constraints on the EBL that other authors have derived using high-energy data. In Section 4, we compare our EBL model with several others that have been proposed using a variety of techniques in recent years. We conclude in Section 5 with a summary of results and a discussion of how current and future high-energy observations will continue to constrain the EBL.

2 MODEL

This section summarizes the SAM that is used to predict the EBL in this work. This model is based upon the models that were first presented in Somerville & Primack (1999) and Somerville et al. (2001), with significant new ingredients as described in Somerville et al. (2008, hereafter S08). Readers should refer to SGPD12, as well as S08, for details.

2.1 Galaxy formation

We assume a standard ΛCDM universe and a Chabrier (Chabrier 2003) stellar initial mass function (IMF) that does not evolve in redshift. The model presented in this work uses cosmological parameters based on *WMAP*5, including a power spectrum normalization of $\sigma_8 = 0.82$, a value that is intermediate between the previous findings of *WMAP*1 and *WMAP*3. This value is within 1σ of the recently published value from *WMAP7* of 0.809 ± 0.024 (Komatsu et al. 2011). The SAMs used here are based on Monte Carlo realizations of dark matter halo merger histories calculated using the modified Press–Schechter (Sheth & Tormen 1999) and extended Press–Schechter methods.

Star formation occurs when gas is accreted by the galaxy and becomes available after cooling via atomic processes. Feedback from supernovae can heat and eject the cold gas within the galaxy. This gas will either be deposited in the hot reservoir connected with the dark matter halo, or returned to the IGM, depending on the wind velocity relative to the virial velocity of the halo. Star formation in our model occurs in two regimes, quiescent star formation in isolated galaxies and merger-driven starbursts. The former is treated using a recipe based on the empirical Schmidt–Kennicutt relation (Kennicutt 1989; Kennicutt et al. 1998). Mergers drive gas deep into galactic nuclei, fuelling black hole growth which power AGN-driven winds. Supermassive black holes can also produce radio jets that heat the hot halo gas and may eventually shut off cooling and eventually lead to a cessation of star formation. This 'quenching' of star formation tends to occur in massive galaxies, which are able to build massive black hole, and which are accreting gas from hot, tenuous haloes rather than via cold dense filaments.

The chemical enrichment and star formation history of each galaxy are used to predict the total emission spectrum. We have adopted the Bruzual & Charlot (2003) stellar population models in this work.

2.2 Dust extinction and reemission

Light emitted by stars can be absorbed and reemitted by dust. In the SAM, dust is modelled as a two-component distribution, using a modified version of the prescription of Charlot & Fall (2000), which treats separately the dense dust in giant molecular clouds that contain newborn stars and the much more diffuse cirrus in the interstellar medium (ISM). Extinction from the ISM component is proportional to the density and metallicity of cold dust, and a slab geometry is assumed. Stars younger than 10^7 yr are enshrouded in a cloud of dust with optical depth $\tau_{\mathrm{BC},V} = \mu_{\mathrm{BC}}\,\tau_{V,0}$, where $\mu_{\mathrm{BC}} = 3$ and $\tau_{V,0}$ is the face-on, V-band extinction of the ISM component. To calculate extinction at other wavelengths, we have assumed a starburst attenuation curve (Calzetti et al. 2000) for the diffuse dust component and a power-law extinction curve $A_\lambda \propto (\lambda/5500\ \text{Å})^n$, with $n = 0.7$, for the birth clouds (Charlot & Fall 2000).

We consider two possible normalizations for the extinction recipes. In our '*WMAP*5+fixed' model, parameters are constant at all redshifts, and are adjusted to match observed relations between UV and IR luminosity for nearby galaxies. However, as discussed in SGPD12, we have found that this model has difficulty reproducing luminosity functions at higher redshift in the UV and optical bands. Motivated by this finding, we have created an 'evolving' model with redshift-dependent parameters tuned to match the observed UV and optical luminosity functions at all redshifts where they have been measured. In this model, total dust extinction is scaled by a factor $(1 + z)^{-1}$ at non-zero redshifts, and the opacity and lifetime of molecular clouds is scaled by a factor z^{-1} above redshift 1. Because this evolving dust model is found to be more successful at matching high-redshift data, we favour this model and will refer to it as the 'fiducial' variant in the next section.

The reemission of IR light by the dust due to thermal and PAH emission is estimated in our model using templates that describe the spectra of galaxies from the mid-IR to submillimetre as a function of the total IR luminosity, and are based on observations of galaxies in the local universe. Energy absorbed by dust from direct starlight is redistributed in the infrared according to a prescribed SED. These templates are embedded in our SAM, and account for emission at wavelengths from a few microns to the submillimetre, including the emission and absorption lines appearing in the PAH region.

The dust emission templates we have used here are described in Rieke et al. (2009, hereafter R09), and are based on observations of 11 local LIRGs and ULIRGs combined with lower luminosity local systems. A comparison of these templates with those of Devriendt, Guiderdoni & Sadat (1999), Devriendt & Guiderdoni (2000), which were used in Primack et al. (2001, 2005, 2008), is available in SGPD12. Being observationally based, these templates suffer to some extent from starlight contamination at short wavelengths, and

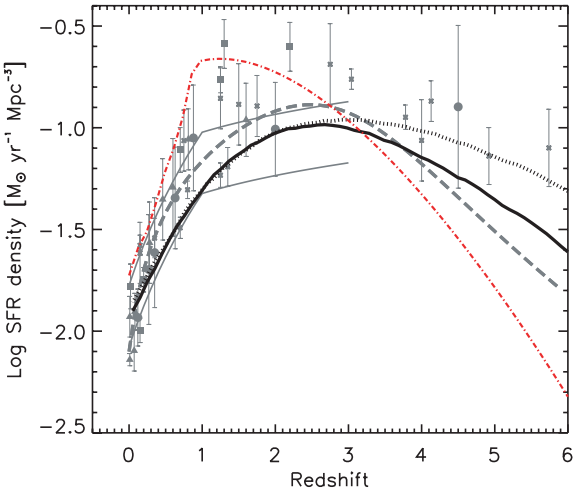

Figure 1. The SFR density in each of the two SAMs over cosmic time. The solid and dotted black curves are the predictions from our *WMAP*5 and CΛCDM models, respectively. The dash–dotted red line is the SFR density inferred from the model of D11, which has been converted to a Chabrier IMF. Grey data points are from a compilation presented in S08; and the dashed line is the estimate of Hopkins & Beacom (2006).

there is also a discontinuity in the galactic SEDs where the templates are joined with our stellar synthesis models, at about 4 μm. In the wavelength range of 2–5 μm we have attempted to compensate for these problems by fitting a power-law extrapolation to the templates. The overall effect of this change to the integrated background light that we will present in the next section is minimal.

3 RESULTS

3.1 Overview of astrophysical results

In this section, we present results for the evolving background light predicted by our SAMs. In addition to our fiducial model, which uses a *WMAP*5 cosmology combined with the evolving dust model and R09 templates described in the last section, we will also show results using employing the 'fixed' dust absorption model to facilitate comparison with our older work. Results from our CΛCDM model will also be shown when relevant. As in the previous section, much of the material here is a review of key results from SGPD12, and readers should refer to this work for further detail. We will also compare with the work of D11, a more observationally driven model that provides a useful contrast to our theoretical approach. Predictions for the evolving EBL and gamma-ray opacity in the fiducial and fixed models are available online in tabulated form.[1]

3.1.1 Star formation and luminosity density history

The global SFR density arising in our *WMAP*5 and CΛCDM models is shown in Fig. 1, along with observational estimates obtained using a variety of tracers. Our model makes predictions that are in agreement with the bulk of data for $z < 1$, and tend to be slightly lower than observed at $z \sim 2$. All measured SFRs are subject to significant uncertainties, as seen in the scatter in results for the plotted data. Uncertainties in dust extinction impact all results relying on UV luminosity. Measurements of Hα and other spectral lines must take into account extinction as well as metallicity effects. Other authors have attempted to measure SFRs based on 24 μm and other mid-IR observations of warm dust. These results can be affected by AGN contamination, as well as PAH features that move in and out of the instrument bandpass with changing redshift. All of these uncertainties grow with increasing redshift, where our knowledge of dust distribution and galaxy SEDs becomes less reliable. The SFR density inferred from the UV and IR luminosity densities of D11 is also shown here. The larger value predicted in this work relative to ours is due to the considerably higher far-IR emission in D11; predictions in the optical and near-IR are similar. Above redshift 1, SFR density predictions from D11 are affected by the assumption made about the evolution of different galaxy spectral types.

The luminosity density in our models is predicted by summing over the emission from individual galaxies. Results for total galactic emissivity as a function of wavelength and redshift are shown in the right-hand panel of Fig. 2. In the left-hand panel we show predicted luminosity density in the local universe, compared to constraints at a number of wavelengths. The local luminosity density has been extremely well measured in the optical and near-IR by large-scale surveys such as Sloan Digital Sky Survey (SDSS) and 2-Micron All Sky Survey (2MASS), and this provides a strong constraint on any model of the galaxy population. At longer wavelengths, we show how our models fit the local data at IR wavelengths, including data from *IRAS* and Submillimetre Common-User Bolometer Array (SCUBA).

We have also compared our model with observational estimates of the evolving luminosity density at a number of different redshifts (Fig. 3). The peak emissivity redshift in our model changes depending on the wavelength considered. At UV bands, the emission closely follows the SFR, which peaks at $z \approx 2.5$ in our *WMAP*5 model and $z \approx 3$ in the CΛCDM model. Longer wavelengths include significant contributions from progressively more evolved stellar populations, and therefore peak at later times. Recent evolutionary surveys such as DEEP2 and COMBO-17 allow us to compare the evolution of galaxy emissivity against accurate luminosity density data in several bands. Emissivity in the UV (1500 and 2800 Å) has been seen to increase out to nearly $z = 2$ (Dahlen et al. 2007). Note the large discrepancy between the evolving and fixed dust attenuation models at high redshift in the *B* band and UV; in the evolving model much less attenuation of starlight occurs in early star-forming galaxies. At high redshift our fiducial UV predictions are somewhat higher than the measurements of Bouwens et al. (2007); this is largely due to a substantial contribution to the total emissivity from faint galaxies which have very little extinction in our evolving dust model.

In the *B* band, Dahlen et al. (2005) find that emission increases out to at least $z = 1$; this paper makes the claim that emissivity in the *B* and *R* bands is consistent with being flat in the interval $1 < z < 2$. Results at the higher redshifts could be sensitive to the faint end slope assumed in calculating the luminosity density. In the *K* band we match well the local luminosity measurement of Kochanek et al. (2001). Available data at higher redshifts seem to suggest a falloff in emissivity beginning at about $z \gtrsim 1$ which we do not find in our models. As discussed in SGPD12, our model does seem to overpredict the *K*-band luminosity of galaxies at and below L^*, beginning at redshifts 1–2. A corresponding overproduction of near-IR flux is not seen in the local luminosity density or *K*-band counts.

3.1.2 Local EBL flux and discrete sources

As mentioned in the Introduction, measurements of the local ($z = 0$) EBL generally fall into two categories: direct sky photometry

[1] http://physics.ucsc.edu/~joel/EBLdata-Gilmore2012

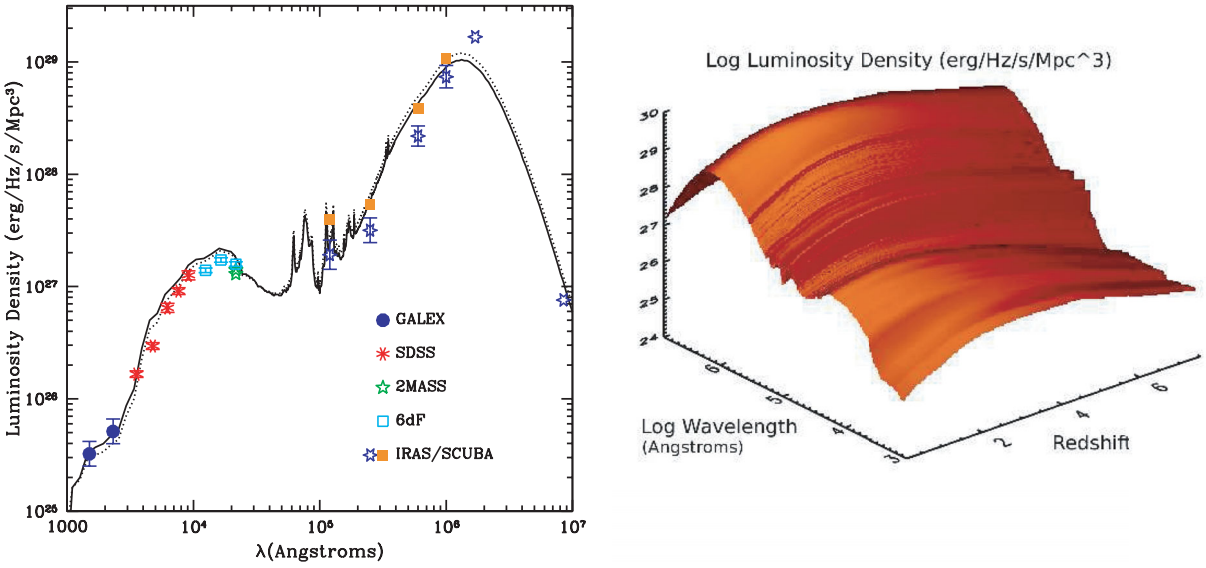

Figure 2. Left: the luminosity density of the local universe. The solid black line is the *WMAP*5 model, and the dotted line is the CΛCDM model. Data at a number of wavelengths are shown from *GALEX* (blue circles), SDSS (red stars; Montero-Dorta & Prada 2009), 6dF (light blue squares; Jones et al. 2006), 2MASS (green stars; Cole et al. 2001; Bell et al. 2003). In the mid- and far-IR, the orange squares are from *IRAS* (Soifer & Neugebauer 1991), while blue stars are from an analysis of local emissivity using data from *IRAS*, *ISO* and SCUBA (Takeuchi et al. 2001). Right: three-dimensional representation of the evolution of the luminosity density in our *WMAP*5 model as a function of wavelength and redshift.

and integrated counts of galaxies. Direct measurements provide an absolute measurement of the background light without regard to the sources responsible, but require subtraction of foreground sources present in the Milky Way and our Solar system in order to isolate the extragalactic signal. Integration of galaxy counts (galaxies per unit sky area at a given magnitude) is a way to set firm lower limits on the EBL, although the degree to which these measurements converge on the true value often remains controversial. The flux from faint sources will converge mathematically if the slope of the counts plotted on a log number versus flux diagram is flatter than unity, or in terms of magnitudes if $\alpha < 0.4$, for $\ln(N) \propto \alpha\, m$. As expounded by Bernstein (2007), photometry of faint galaxies is fraught with difficulty in untangling the faint galactic fringes from the background, and it is possible to miss 50 per cent or more of the light associated with extended sources in simple aperture photometry.

Large-scale surveys such as the SDSS, the 6-degree Field survey (6dF) and the 2MASS have provided us with an accurate accounting of the galaxies in the local universe, and surveys with the *HST* have complemented this data with extremely deep counts. Satellite instruments such ISOCAM, IRAC and MIPS provide data in the mid- and far-IR. A detailed presentation of galaxy number counts in our models compared with data can be found in SGPD12.

Our prediction for the local EBL is generally in agreement with lower limits from integrated number counts. In the UV, limits from Gardner, Brown & Ferguson (2000) are considerably higher than the measurement from *GALEX* (Xu et al. 2005). This may be explained by the former's use of data from the balloon-based FOCA experiment to find bright counts, which were in disagreement with those from *GALEX* at several magnitudes. Preliminary Herschel counts data from Berta et al. (2010) set only a weak lower limit on the far-IR background peak, and the author acknowledges that only about half the total IR background is likely being resolved.

Absolute measurements of the EBL require the removal of foreground sources, including stars, ISM emission and sunlight reflected from dust in the inner Solar system (often called 'zodiacal' light). The most robust direct measurements of the IR background to date come from DIRBE and FIRAS instruments on the *Cosmic Background Explorer* (*COBE*) satellite, though they are still fraught with uncertainty in sky subtraction (see fig. 2 in Hauser & Dwek 2001). The near-IR flux has been calculated from DIRBE observations by a variety of authors (Gorjian, Wright & Chary 2000; Wright & Reese 2000; Cambrésy et al. 2001; Wright 2001; Levenson, Wright & Johnson 2007) using foreground source subtraction techniques and modelling of the zodiacal light, and has generally yielded high estimates in this range compared to number counts. Another notable attempt to measure the near-IR background was Levenson & Wright (2008), which used IRAC data to calculate the best-fitting flux at 3.6 μm using a profile-fit to estimate the light from the unobservable faint fringes of galaxies. These results were 70 per cent higher than those of the aperture method of Fazio et al. (2004), highlighting the large uncertainties that galaxy fringe issues can bring to EBL measurement.

The present-day EBL obtained in each of our models is shown in Fig. 4. We also show results from D11 for comparison. The local EBL is calculated by integrating over the luminosity density at all wavelengths beginning at $z = 7.5$, and accounting for the redshifting and dilution of photons as the universe expands. The EBL at a redshift z_0 and frequency ν_0 in proper coordinates can be written as (Peebles 1993)

$$J(\nu_0, z_0) = \frac{1}{4\pi} \int_{z_0}^{\infty} \frac{\mathrm{d}l}{\mathrm{d}z} \frac{(1+z_0)^3}{(1+z)^3}\, \epsilon(\nu, z)\, \mathrm{d}z, \quad (1)$$

where $\epsilon(\nu, z)$ is the galaxy emissivity at redshift z and frequency $\nu = \nu_0(1+z)/(1+z_0)$, and $\mathrm{d}l/\mathrm{d}z$ is the cosmological line element, which is

$$\frac{\mathrm{d}l}{\mathrm{d}z} = \frac{c}{(1+z)H_0} \frac{1}{\sqrt{\Omega_\mathrm{m}(1+z)^3 + \Omega_\Lambda}} \quad (2)$$

for a flat ΛCDM universe. We assume here that the EBL photons evolve passively after leaving their source galaxies and are

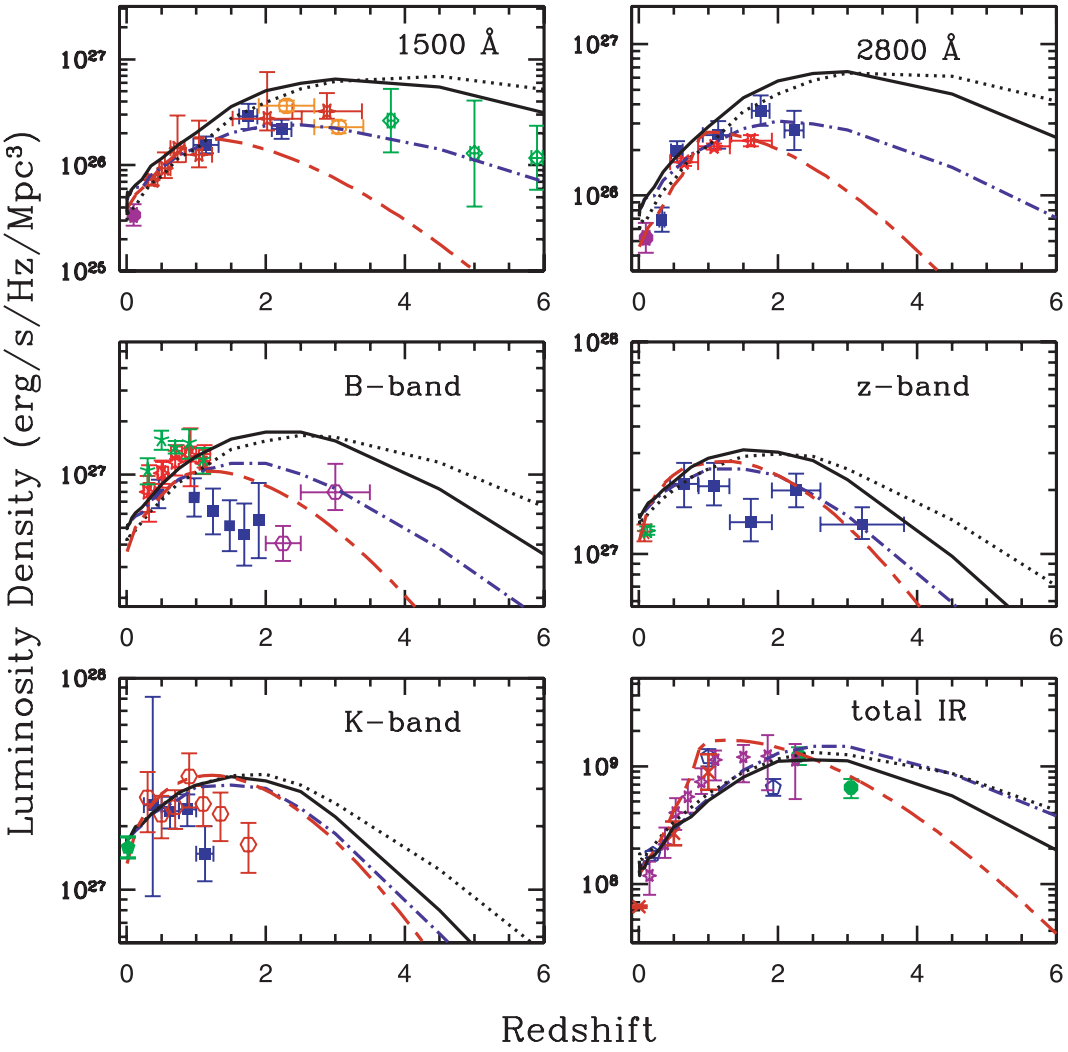

Figure 3. The luminosity density (integrated luminosity function of sources within a given redshift range) in our models versus redshift at 1500, 2800 Å, and in the *B*, *z* and *K* bands (approximately 4500, 9130 Å and 2.2 μm, respectively). The final panel on the lower right shows the total amount of energy that is absorbed and reradiated by dust at IR energies; units on the *y*-axis for this panel are solar luminosities per Mpc^3. The solid black line is our *WMAP*5 prediction with evolving dust, and the dotted line are prior results from our CΛCDM model. Dash–dotted violet shows the predictions from our *WMAP*5 model using fixed dust attenuation parameters. The long–short dashed red line is the prediction of D11. Observational data shown here are as follows. 1500 Å: blue squares are from Dahlen et al. (2007), red stars are from Schiminovich et al. (2005), green stars are from Bouwens et al. (2007) and orange circles are from Reddy et al. (2008). The solid purple circle is a local measurement with *GALEX* by Wyder et al. (2005). 2800 Å: blue squares and the purple circle are again from Dahlen et al. (2007) and Wyder et al. (2005), respectively. Red stars are from Gabasch et al. (2006). *B* band: blue squares are from Dahlen et al. (2005). DEEP and COMBO-17 data from Faber et al. (2007) are shown as red stars and open red squares, respectively (these are very similar). This Combo-17 data is an update to that originally presented in Wolf et al. (2003), and we show the original points as green stars. The work of Marchesini et al. (2007) is shown as open purple hexes. *z* band: local measurements are provided by Montero-Dorta & Prada (2009) (red) and Blanton et al. (2003) (green). Blue squares are from Gabasch et al. (2006). *K* band: the local determination is from Kochanek et al. (2001). High-redshift data are from Barro et al. (2009) (blue squares) and Arnouts et al. (2007) (open red circles). Total IR luminosity: observational estimates of the IR emissivity are from Caputi et al. (2007) (open blue pentagons), Reddy et al. (2008) (green circles), Rodighiero et al. (2010) (purple stars) and Le Floc'h et al. (2005) (red crosses).

not affected by any further interactions except for cosmological redshifting. This is an acceptable approximation for photons at energies below the Rydberg energy of 13.61 eV. Photons above this energy are strongly attenuated by neutral hydrogen when leaving their galaxy of origin. At higher energies, photons are also capable of interacting with residual neutral hydrogen and, if sufficiently energetic, neutral and singly ionized helium in the IGM. The effect of these processes on the ionizing EBL is the topic of our previous work in Gilmore et al. (2009). The total flux of the integrated EBL as well as the contributions from the optical–near-IR and far-IR peaks and the mid-IR valley for each model are shown in Table 1.

3.1.3 *Evolution of the background flux*

A correct determination of gamma-ray opacity at distances beyond the very nearby universe, $z > 0.05$, requires accounting for the redshift-dependent evolution of the background at all wavelengths. The sharply increasing SFR density from $z = 0$ back to $z \sim 2$, combined with the $(z+1)^4$ evolution of proper flux in redshift means that the background was considerably more powerful in the recent past, a fact that can only be neglected in gamma-ray attenuation calculations for the closest extragalactic sources. With observations of VHE extragalactic sources now stretching out to redshifts of over

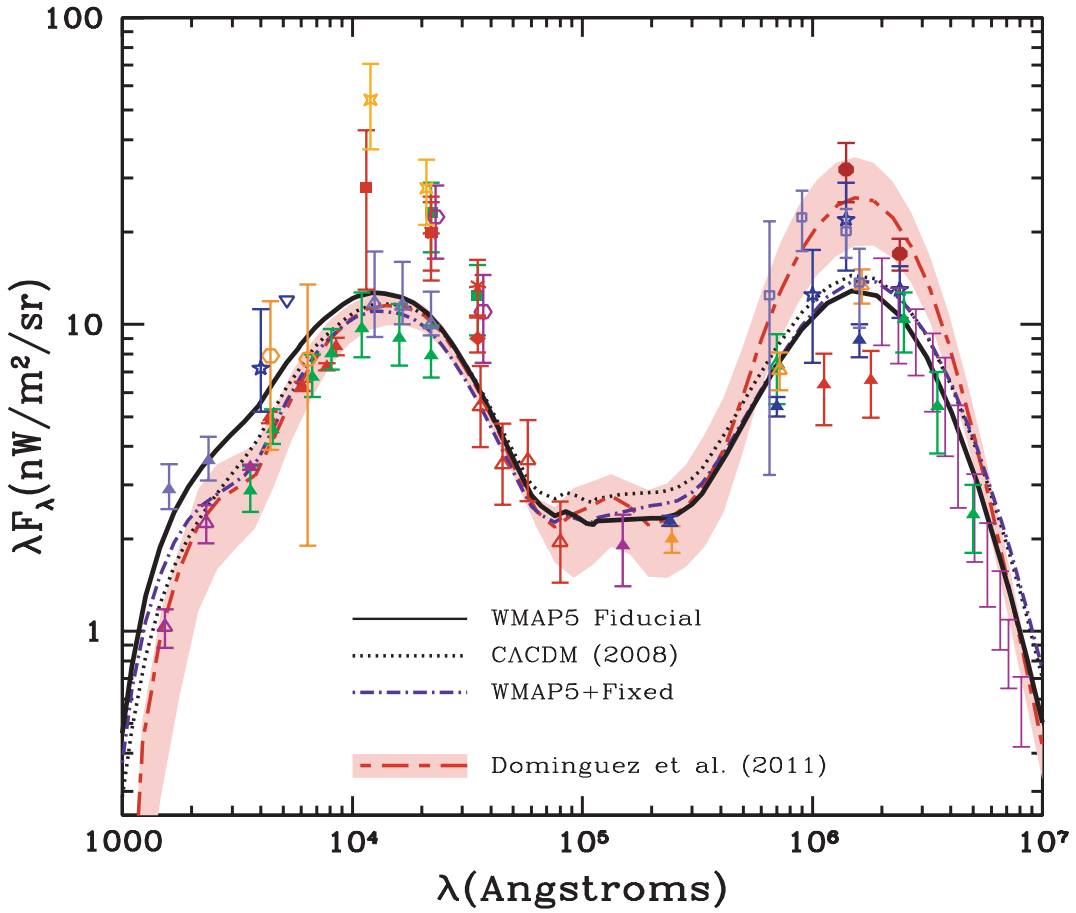

Figure 4. The predicted $z = 0$ EBL spectrum from our fiducial *WMAP5* model (solid black) and *WMAP5*+fixed (dash–dotted violet) dust parameters, and CΛCDM (dotted black) models, compared with experimental constraints at a number of wavelengths. D11 is shown for comparison in dashed–dotted red with the shaded area indicating the uncertainty region. Data: upward pointing arrows indicate lower bounds from number counts; other symbols are results from direct detection experiments. Note that some points have been shifted slightly in wavelength for clarity. Lower limits: the blue–violet triangles are results from *HST* and Space Telescope Imaging Spectrograph (STIS; Gardner et al. 2000), while the purple open triangles are from *GALEX* (Xu et al. 2005). The solid green and red triangles are from the *Hubble Deep Field* (Madau & Pozzetti 2000) and *Ultra Deep Field* (Dolch & Ferguson, in preparation), respectively, combined with ground-based data, and the solid purple triangle is from a measurement by the Large Binocular Camera (Grazian et al. 2009). In the near-IR *J*, *H* and *K* bands, open violet points are the limits from Keenan et al. (2010). Open red triangles are from IRAC on *Spitzer* (Fazio et al. 2004), and the purple triangle at 15 μm is from ISOCAM (Hopwood et al. 2010) on *ISO*. The lower limits from MIPS at 24, 70 and 160 μm on *Spitzer* are provided by Béthermin et al. (2010) (solid blue) and by Chary et al. (2004), Frayer et al. (2006) and Dole et al. (2006) (solid gold, open gold and open green, respectively). Lower limits from Herschel number counts (Berta et al. 2010) are shown as solid red triangles. In the submillimetre, limits are presented from the BLAST experiment (green points; Devlin et al. 2009). Direct detection: in the optical, orange hexagons are based on data from the Pioneer 10/11 Imaging Photopolarimeter (Matsuoka et al. 2011), which are consistent with the older determination of Toller (1983). The blue star is a determination from Mattila et al. (2011), and the triangle at 520 nm is an upper limit from the same. The points at 1.25, 2.2 and 3.5 μm are based upon DIRBE data with foreground subtraction: Wright (2001, dark red squares), Cambrésy et al. (2001, orange crosses), Levenson & Wright (2008, red diamond), Gorjian et al. (2000, purple open hexes), Wright & Reese (2000, green square) and Levenson et al. (2007, red asterisks). In the far-IR, direct detection measurements are shown from DIRBE (Schlegel, Finkbeiner & Davis 1998; Wright 2004, solid red circles and blue stars) and FIRAS (Fixsen et al. 1998, purple bars). Blue–violet open squares are from IR background measurements with the *AKARI* satellite (Matsuura et al. 2011).

Table 1. The integrated flux of the local EBL in our models (*WMAP5* with evolving and fixed dust parameters, and the CΛCDM model) and the model of D11. Units are nW m^{-2} sr^{-1}.

Wavelength range	*WMAP5* (fiducial)	*WMAP5*+fixed	CΛCDM	D11
Optical–near-IR peak (0.1–8 μm)	29.01	24.34	26.15	24.47
Mid-IR (8–50 μm)	4.89	5.16	5.86	5.24
Far-IR peak (50–500 μm)	21.01	22.94	24.08	39.48
Total (0.1–500 μm)	54.91	52.44	56.09	69.19

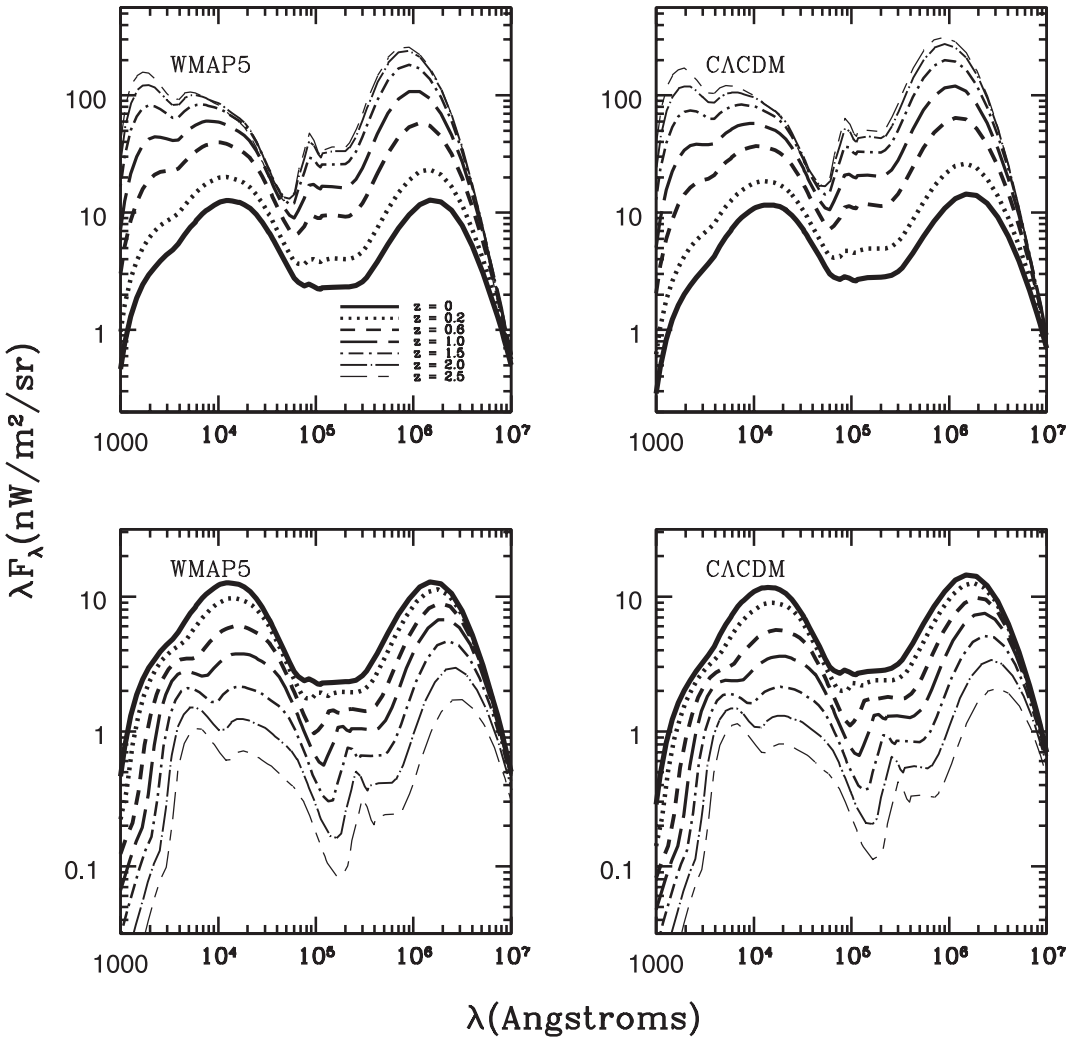

Figure 5. The history of the EBL in each of our models. The top two plots show the background flux at past redshifts in the *WMAP*5 fiducial (left) and CΛCDM (right) models in standard units. Redshifts shown include $z = 0$ (solid), $z = 0.2$ (dotted), $z = 0.6$ (short dashed), $z = 1$ (long dashed), $z = 1.5$ (dot–short dashed), $z = 2$ (dot–long dashed) and $z = 2.5$ (long and short dashed); also see the key in the upper left-hand panel. The bottom two plots show the same quantities, but now evolved to present-day (comoving), allowing easy comparison of the EBL in place at a particular time compared to the total in existence at $z = 0$.

0.5, it is important in comparing different realizations of the EBL that we focus not only on the flux at $z = 0$ but at higher redshifts as well, where behaviour may be quite different in a given model depending on how galaxies evolve. We show how the background develops in our models in two ways in Fig. 5. The top panels show the proper EBL SED from different redshifts in the rest frame, for each of our models. The bottom panels show the comoving EBL at those same redshifts; this is the background that would be seen today if all galaxy emissivity had been shut off below the indicated redshift. It can be seen in the top plots that the EBL photon density was considerably higher in the past at all wavelengths. The most striking increases from present day levels are in the mid- and far-IR, and in the UV.

Complementary to Fig. 5, in Fig. 6 we show how the photons populating the IR EBL at various wavelengths today were produced as a function of redshift. As expected from our knowledge of obscured starbursting galaxies at high redshift, the mid- and far-IR parts of the EBL came into existence considerably sooner than the photons that are part of the optical–near-IR peak today. Our results are in reasonable agreement with a recent survey of submillimetre galaxies (Devlin et al. 2009), which has found that half of the background radiation at 250 μm is produced at $z > 1.2$, with this fraction increasing at longer wavelengths. The results for the *WMAP*5 and CΛCDM models are qualitatively similar, however, due to earlier star formation in the latter, a greater percentage of photons were in place at a given redshift for all wavebands relative to the *WMAP*5 model. Because the measurements shown here are unavoidably incomplete at high redshift, the fact that our models overpredict the fraction of light in place at early times is not necessarily in conflict with these results.

The rapid increase in flux at all wavelengths with increasing redshift means that the attenuation per unit distance increases a corresponding amount. Therefore, gamma-rays from more distant blazars suffer more attenuation than might be expected from the local EBL flux. In addition, the SED shape of the EBL changes, so a simple z-dependent scaling factor is not sufficient to allow accurate predictions of spectral modification for the more distant sources.

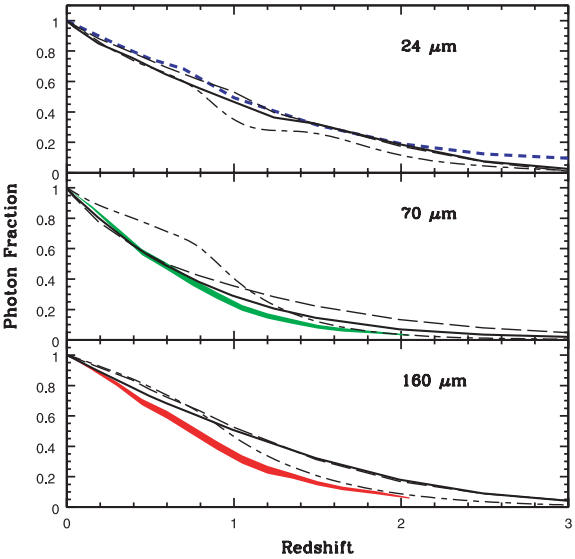

Figure 6. Build-up of the present-day background photon population in three different bands (observed frame), showing the fraction of the present-day comoving number density in place at a given redshift. Solid black is our fiducial *WMAP*5 model, dashed is the *WMAP*5+fixed and dash–dotted is the model of D11. We have compared against the measurements of Le Floc'h et al. (2009) (blue) at 24 μm and Jauzac et al. (2011) at 70 (green) and 160 μm (red). For the latter two, the extent of the shaded region is the 1σ error bound.

3.2 Gamma-ray attenuation

The process of photon–photon scattering to electron–positron pairs is well understood from quantum electrodynamics. The basic kinematic requirement for this process is that there must be sufficient energy in the centre-of-mass frame of the two-photon system to create the pair. Including the effect of interaction angle as measured in the cosmological frame, this can be written as

$$\sqrt{2E_1E_2(1-\cos\theta)} \geq 2m_ec^2, \tag{3}$$

where E_1 and E_2 are the photon energies and θ is the angle of incidence. We are interested here in cases where the target background photon has energies from the far-IR ($\gtrsim 10^{-2}$ eV) to the Lyman limit ($\lesssim$13.6 eV). The corresponding gamma-ray energies are therefore in the TeV or GeV range. We can rewrite equation (3) to define the minimum threshold energy $E_{\rm th}$ for a background photon to interact with a gamma-ray of energy E_γ,

$$E_{\rm th} = \frac{2m_e^2c^4}{E_\gamma(1-\cos\theta)}. \tag{4}$$

The cross-section for this process is (Gould & Schreder 1967; Madau & Phinney 1996)

$$\sigma(E_1,E_2,\theta) = \frac{3\sigma_{\rm T}}{16}(1-\beta^2) \times \left[2\beta(\beta^2-2)+(3-\beta^4)\ln\left(\frac{1+\beta}{1-\beta}\right)\right], \tag{5}$$

where

$$\beta = \sqrt{1-\frac{2m_e^2c^4}{E_1E_2(1-\cos\theta)}}, \tag{6}$$

and $\sigma_{\rm T}$ is the Thompson scattering cross-section.

The cross-section is maximized for centre-of-mass energies of approximately twice the threshold energy $2m_ec^2$, and falls approximately as inverse energy for $E \gg E_{\rm th}$. If we also account for θ, we find that the likelihood of absorption is maximized for photons at about four times the absolute threshold energy, with one factor of 2 from σ and another in going from $\theta = \pi$ ('head-on' configuration) to the most probable angle of interaction $\theta \approx \pi/2$. If we assume $\theta = \pi/2$, then we can define the characteristic energy or wavelength for the background photons that will most strongly affect a gamma-ray of energy E_γ as

$$E_{\rm bg} = \frac{4m_e^2c^4}{E_\gamma} = 1.044\left(\frac{\rm TeV}{E_\gamma}\right)\ {\rm eV}, \tag{7}$$

or equivalently,

$$\lambda_{\rm bg} = 1.188\left(\frac{E_\gamma}{\rm TeV}\right)\ \mu{\rm m}. \tag{8}$$

Gamma-rays at a rest-frame energy above 1 TeV are most attenuated by the near- and mid-IR range of the EBL, while those in the 200 GeV to 1 TeV regime are sensitive to light in the near-IR and optical peak in the EBL SED. Below 200 GeV it is mainly UV photons that have sufficient energy to cause the pair production interaction. Below 19 GeV only background photons with energies above the Lyman limit of 912 Å have sufficient energy to interact at any angle in the rest frame, and there is little attenuation due to the paucity of such photons (Oh 2001; Gilmore et al. 2009).

To calculate the optical depth for a gamma-ray observed at energy E_γ, we perform the integral along the line of sight to the target at redshift z,

$$\tau(E_\gamma,z_0) = \frac{1}{2}\int_0^{z_0}{\rm d}z\,\frac{{\rm d}l}{{\rm d}z}\int_{-1}^{1}{\rm d}u\,(1-u) \times \int_{E_{\rm min}}^{\infty}{\rm d}E_{\rm bg}\,n(E_{\rm bg},z)\,\sigma(E_\gamma(1+z),E_{\rm bg},\theta). \tag{9}$$

Where we have

$$E_{\rm min} = E_{\rm th}\,(1+z)^{-1} = \frac{2m_e^2c^4}{E_\gamma(1+z)(1-\cos\theta)}$$

to account for the redshifting of the gamma-ray energy. Here $n(E_{\rm bg}, z)$ is the proper density of target background photons as a function of energy $E_{\rm bg}$ and redshift z, and u is shorthand for $\cos\theta$. dl/dz is the cosmological line element, equation (2).

For nearby sources, $z \lesssim 0.05$, it is sufficient to use the local EBL density $n(E_{\rm bg}, z = 0)$. However, as we saw in Fig. 5, both the total power and SED of the EBL vary strongly with redshift, and in general it is therefore necessary to understand the evolution of the background to correctly compute gamma-ray opacities. The rapid increase in flux at all wavelengths with increasing redshift to $z \gtrsim 2$ means that the attenuation per unit proper distance increases a corresponding amount. This effect means that gammas from more distant blazars suffer more attenuation than might be expected from the local EBL flux. In addition, the functional form of the EBL changes, so a simple z-dependent scaling factor is not sufficient to allow accurate predictions of spectral modification for the more distant sources. Using the line-of-sight integral, equation (9), we show in Fig. 7 the optical depth versus gamma-ray energy for a variety of redshifts. A more general way to show EBL attenuation is to plot the 'attenuation edge' redshift where the optical depth reaches a certain value as a function of gamma-ray energy, and this is presented out to high redshift for three values of τ in Fig. 8. This shows how telescopes with lower energy thresholds will allow us to peer deeper into the universe. See Gilmore et al. (2009) for a similar plot extending to lower gamma-ray energies and higher redshift.

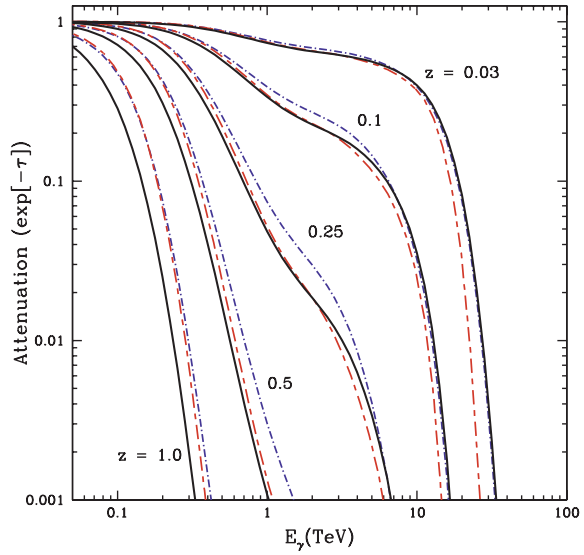

Figure 7. The attenuation $e^{-\tau}$ of gamma-rays versus gamma-ray energy, for sources at $z = 0.03$, 0.1, 0.25, 0.5 and 1. Results are compared for our fiducial *WMAP*5 (solid) and *WMAP*5+fixed (dash–dotted violet) models, as well as the model of D11 (red dash–dotted). Increasing distance causes absorption features to increase in magnitude and appear at lower energies. The plateau seen between 1 and 10 TeV at low redshift is a product of the mid-IR valley in the EBL spectrum.

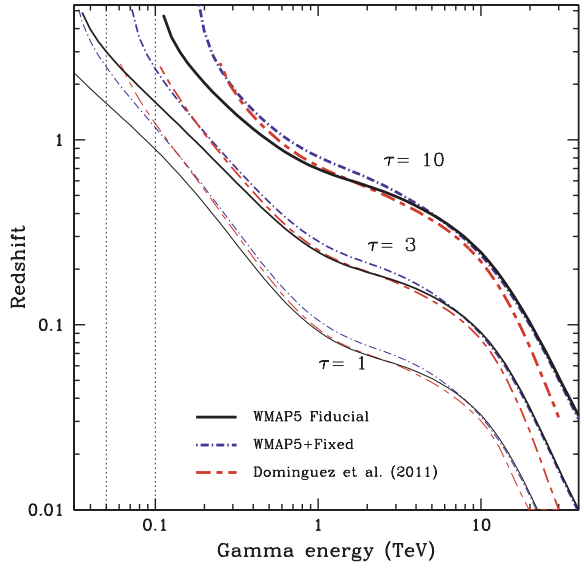

Figure 8. The gamma-ray attenuation edges for the *WMAP*5 (solid black) and *WMAP*5+fixed (dash–dotted violet) models and model of D11 (red dash–dotted). The curves show the redshift at which the pair production optical depth τ reaches the indicated value for a particular observed gamma-ray energy. The groups of curves from lower left to upper right are the contours for $\tau = 1$, 3 and 10. We have included thin lines to guide the eye at 50 and 100 GeV.

3.3 Results for TeV blazars

Today, exploration in the VHE (30 GeV to 30 TeV) regime is led by >10-m-class imaging atmospheric Cherenkov telescopes (IACTs) including the Very Energetic Radiation Imaging Telescope Array System (VERITAS; Maier et al. 2008), High Energy Stereoscopic System (HESS; Hinton 2004) and Major Atmospheric Gamma-Ray Imaging Cherenkov (MAGIC; Cortina 2005) experiments, and by the Large Area Telescope (LAT) instrument on the *Fermi* gamma-ray space telescope (Atwood et al. 2009) and also AGILE (Tavani et al. 2008).

The *Fermi* LAT spends most of its time in an-all sky survey mode, and with its large area of view is therefore an ideal instrument for finding high-energy sources. The 11-month source catalogue lists 685 high-energy sources associated with blazar candidates (Abdo et al. 2010a). While the *Fermi* LAT has an energy range of 20 MeV to ∼300 GeV, it has a much smaller effective area than the current generation of ground-based instruments, and data from the instrument is therefore most useful for our purposes at energies below the threshold of these IACTs, 50–100 GeV. A detailed analysis of the EBL constraints available from all *Fermi* observations of blazars and gamma-ray bursts (GRBs) to date was the subject of a recent paper by the *Fermi* collaboration, Abdo et al. (2010b). Current limits on the EBL available from *Fermi* observations do not constrain the UV flux predicted in Gilmore et al. (2009) or in the models presented here.

In this section and the following section, we will focus on the effect of the optical–IR EBL on AGN-type sources by IACTs at $\gtrsim$100 GeV. Ground-based detectors searching above 100 GeV have identified 37 extragalactic AGN-like sources at the time of this writing, including 32 BL Lac objects, radio galaxies M87 and Centaurus A, and the flat-spectrum radio quasars 3C 279, PKS 1510−08 and PKS 1222+21. With the exception of the radio galaxies these objects are all blazars, accreting AGN which generate tightly beamed relativistic jets that are oriented at a small angle relative to our line of sight. While they account for the large majority of detected sources above 100 GeV, BL Lac objects are themselves only a small subset (∼20 per cent) of all blazar sources, the other 80 per cent being flat spectrum radio quasars like 3C 279.

3.3.1 *Constraints from gamma-ray observations*

While uncertainties and likely variation in the intrinsic spectrum of blazars make it impossible to directly link the observed spectrum to EBL attenuation, it is possible to translate limits on the spectra to EBL constraints. The standard assumption in placing limits on the EBL from individual spectra is that the reconstructed intrinsic spectrum should not have a spectral index harder than 1.5, that is, $\Gamma \geq 1.5$ where $\mathrm{d}N/\mathrm{d}E \propto E^{-\Gamma}$ for photon count N, or alternatively $\mathrm{d}F/\mathrm{d}E \propto E^{-(\Gamma-1)}$ for flux F. This figure comes about both on the basis of experimental observations (no observed VHE spectrum is harder than this value) and theoretical arguments. The standard value for a single-zone synchrotron-self-Compton (SSC) spectrum is $\Gamma = (\alpha + 1)/2$; here $-\alpha$ is the spectral index of the shock-accelerated electrons, which is not harder than 2.0 in most acceleration models with radiative cooling (Aharonian 2001). This can be invalidated by assuming a non-standard spectrum for the electrons; a low energy cut-off in the electron energy will lead to inverse-Compton accelerated photons with an index as low as $\Gamma = 2/3$ (Katarzyński et al. 2006).

The most recent limits on the EBL come from observations of blazars at more distant redshifts ($z > 0.1$) that have been detected by the current generation of ground-based atmospheric Cherenkov telescopes (ACTs). Observation by HESS of two blazars at $z = 0.165$ and 0.186 were used to set limits on the near-IR EBL based on the $\Gamma \geq 1.5$ criterion (Aharonian et al. 2006); in this case the maximal limit was the model of Primack et al. (2001) multiplied by a factor of 0.45. Another paper by the HESS group set constraints from blazar 1ES 0229+200 at $z = 0.1396$ (Aharonian et al. 2007b).

While this blazar is a closer source than the two featured in the 2006 publication, the observed spectrum extended above 10 TeV and therefore probed the background in the mid-IR (equation 8). In this regime, the effect of optical depth on spectral modification is minimal due to the approximate λ^{-1} falloff in EBL flux, which leads to a constant photon density per logarithmic bin, and therefore an approximately constant gamma-ray opacity as a function of energy. The most distant source observed at very high energies at the time of writing is quasar 3C 279 at $z = 0.536$, observed by the MAGIC experiment during a flare in 2006 February (Teshima et al. 2008). The spectrum observed was quite steep, $4.1 \pm 0.7_{\rm stat} \pm 0.2_{\rm sys}$, and extended from about 80 to nearly 500 GeV. An analysis of the spectral modification (Albert et al. 2008) found that there was little room for an EBL flux in the optical higher than one consistent with lower limits from number counts, approximately equivalent to the model of Primack et al. (2005). This paper used a modified version of the 'best-fitting' model from Kneiske et al. (2004) as the upper limit in the optical and near-IR from their finding. An alternative analysis of the spectral deconvolution of 3C 279 by Stecker & Scully (2009) disputed this analysis and argued that the higher EBL of Stecker et al. (2006), Stecker, Malkan & Scully (2007) could still lead to a steep best-fitting spectrum. However, this higher EBL is inconsistent with *Fermi* high-redshift blazar observations at the 5σ level (Abdo et al. 2010b).

Another approach to the problem is to attempt to constrain the EBL by using spectra from several sources simultaneously. Dwek & Krennrich (2005) derived an upper limit at 60 μm by declaring invalid those realizations leading to unphysical intrinsic blazar spectra with sharply rising TeV emissions. More recently, this method was used in Mazin & Raue (2007), who applied constraints from all observed TeV blazars to a large number of possible EBL functional forms created using a spline interpolation across a grid in flux versus wavelength space. The lower bound of the union of excluded models formed an envelope representing the highest possible background that does not violate any constraints. This was done for 'realistic' and 'extreme' bounds of $\Gamma \geq 1.5$ and 2/3, respectively, and provided a limit on the EBL from the optical to the far-IR. The latter case is motivated by the limiting case of a truncation at a low-energy bound for the relativistic electrons responsible for the IC component, see Katarzyński et al. (2006).

In Fig. 9, we show recent upper limits from gamma-ray observations in relation to the $z = 0$ EBL from our models. All of our models are generally in agreement with these bounds across all wavelengths. While our fiducial model does slightly exceed the bounds set by Albert et al. (2008) in the optical, we do not find a conflict with the standard $\Gamma \geq 1.5$ bound in Table 2, and we are within 1σ agreement with the harder spectrum observed by Aleksić et al. (2011b).

It is worth pointing out here that, in general, one should use caution concerning these constraints. These limits on the present-day EBL do not take into account the differences in redshift evolution occurring in different EBL models, which becomes increasingly problematic for more distant sources. Also, as mentioned above the limits from Aharonian et al. (2006) and Albert et al. (2008) assume specific forms for the optical peak of the background SED with variable normalization. The exact normalization of the upper bound is dependent upon this choice. The method used by Mazin & Raue avoids this second issue, but at a cost of more conservative limits resulting from considering a finite grid in flux–wavelength space.

The photon density of the EBL increases with wavelength at almost all energies relevant to gamma-ray attenuation, and therefore the effect on high energy spectra is always a spectral softening.

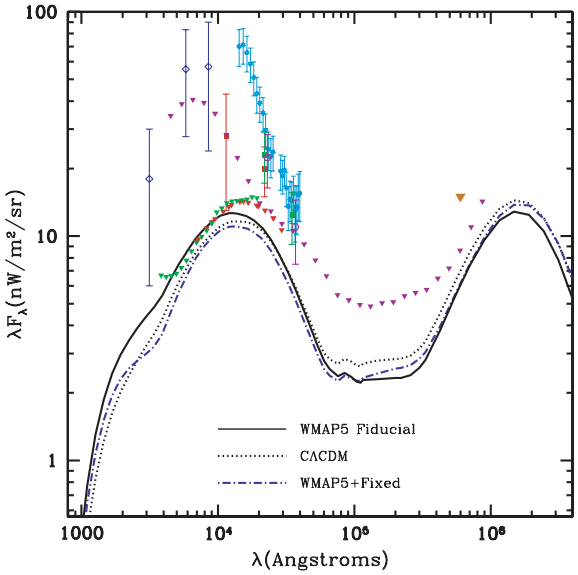

Figure 9. Present-day flux predicted in our EBL models, compared against upper limits from gamma-ray observations. Line types are the same as in Fig. 4. Upper limits are shown as downward-pointing triangles. Red triangles are observations described in Aharonian et al. (2006), and green are from MAGIC observations of 3C 279 (Albert et al. 2008). Other limits shown are the realistic limits of Mazin & Raue (2007) (purple), and the analysis of Dwek & Krennrich (2005) (orange triangle at 60 μm). The reader should consult the text for more details and caveats in interpreting this figure. We also show for comparison many of the high estimates of the optical and near-IR EBL from direct photometry. The open blue diamonds are from Bernstein (2007). The points at 1.25, 2.2 and 3.5 μm are based upon DIRBE data with foreground subtraction: Wright (2001) (dark red squares), Gorjian et al. (2000) (purple open hexes) and Wright & Reese (2000) (green square). The small cyan points are from direct photometry with the *IRTS* satellite (Matsumoto et al. 2005).

However, it is possible that local radiation in the vicinity of a source could have other effects on the spectrum. This is particularly true for FSRQ sources such as 3C 279. As a quasar, 3C 279 is a much more powerful source at optical and UV wavelengths than BL Lac objects. It has therefore been suggested that internal absorption from the broad-line region of the quasar could harden the spectrum by creating an optical depth that decreases with energy over the observed interval (Aharonian, Khangulyan & Costamante 2008c), due to emission in a narrow band of UV wavelengths. An analysis by Tavecchio & Mazin (2009) claimed that while significant internal absorption was likely, only the more extreme models of the broad line region lead to an actual hardening of the intrinsic spectrum, and these models lead to a large decrease in flux from absorption, by a typical factor of $>10^3$. This effect could potentially harden intrinsic spectra emerging from AGN beyond the bounds discussed above, but only in limited extreme cases. More reasonable models of the local radiation fields with less total absorption were found to leave the spectral index softened or unmodified.

3.3.2 Spectral modification of known TeV blazars

We have calculated absorption from each of our EBL realizations in the observed spectra of known blazars that are approximated by power-law functions, and determined the approximate power law of the de-absorbed spectra. The spectra from these objects are not expected to be power laws over large energy ranges. The

Table 2. Reconstruction of the VHE spectral indices of a number of blazars using our two *WMAP*5 EBL realizations. $\Gamma_{\rm obs}$ is the index reported by the given reference at energies between $E_{L\gamma}$ and $E_{H\gamma}$, reported in TeV. These are taken from the reference if explicitly stated, otherwise the highest and lowest data points presented are used. In some cases the highest energy data point presented has large error bars or does not match well with the power-law fit, and we have opted to use the second highest point instead. $\Gamma_{\rm Fiducial}$ and $\Gamma_{\rm Fixed}$ are the average intrinsic indices after de-absorption by our two EBL models, over the range of energies claimed in the detections. Errors on this quantity are the same as in the observed indices, if provided by the author. Plus (+) and minus (−) after the source name are used to signify that the detection was claimed in an abnormally high or low state; readers should consult the references given for further details. Many of these references were taken from Wagner (2008) and also the TeV online catalogue, http://tevcat.uchicago.edu/.

Object ID	Redshift	Reference	Experiment	$E_{L\gamma}$	$E_{H\gamma}$	$\Gamma_{\rm obs}$	$\Gamma_{\rm Fiducial}$	$\Gamma_{\rm Fixed}$
Mrk 421 (+)	0.030	Konopelko et al. (2008)	Whipple	0.2	8.0	2.66	2.46	2.46
Mrk 421	0.030	Aharonian et al. (1999)	HEGRA	0.5	7.0	3.09 ± 0.07	2.88	2.88
1ES 2344+514	0.044	Albert et al. (2007b)	MAGIC	0.14	5.4	$2.95 \pm 0.12 \pm 0.20$	2.71	2.72
Mrk 180 (+)	0.045	Albert et al. (2006c)	MAGIC	0.2	1.5	3.30 ± 0.70	3.04	3.06
1ES 1959+650	0.047	Albert et al. (2006a)	MAGIC	0.18	2.0	2.72 ± 0.14	2.46	2.48
1ES 1959+650 (−)	0.047	Tagliaferri et al. (2008)	MAGIC	0.15	3.0	2.58 ± 0.18	2.34	2.36
1ES 1959+650 (+)	0.047	Daniel et al. (2005)	Whipple	0.38	18.0	$2.78 \pm 0.12 \pm 0.21$	1.95	1.91
BL Lacertae	0.069	Albert et al. (2007c)	MAGIC	0.15	0.9	3.60 ± 0.50	3.25	3.29
PKS 0548−322	0.069	Superina et al. (2008)	HESS	0.2	3.0	2.8 ± 0.33	2.41	2.45
PKS 2005−489	0.071	Aharonian et al. (2005b)	HESS	0.2	2.5	4.0 ± 0.4	3.60	3.63
RGB J0152+017	0.080	Aharonian et al. (2008b)	HESS	0.24	3.8	2.95 ± 0.41	2.48	2.51
W Comae (+)	0.102	Cogan (2008)	VERITAS	0.15	2.8	$3.81 \pm 0.35 \pm 0.34$	3.26	3.32
PKS 2155−304	0.116	Aharonian et al. (2005a)	HESS	0.16	0.70	3.32 ± 0.06	2.74	2.81
H1426+428	0.129	Aharonian et al. (2002)	HEGRA	1.0	6.0	$2.60 \pm 0.60 \pm 0.1$	1.74	1.67
1ES 0806+524	0.138	Acciari et al. (2009a)	VERITAS	0.3	0.7	$3.6 \pm 1.0 \pm 0.3$	2.68	2.79
1ES 0229+200	0.139	Aharonian et al. (2007b)	HESS	0.5	7.0	$2.50 \pm 0.19 \pm 0.10$	1.45	1.40
H2356−309	0.165	Aharonian et al. (2006)	HESS	0.16	1.0	3.06 ± 0.40	2.11	2.23
1ES 1218+304	0.182	Albert et al. (2006b)	MAGIC	0.09	0.63	3.00 ± 0.4	2.28	2.39
1ES 1218+304	0.182	Fortin (2008)	VERITAS	0.16	1.8	$3.08 \pm 0.34 \pm 0.20$	2.02	2.14
1ES 1101−232	0.186	Aharonian et al. (2006)	HESS	0.16	3.3	2.88 ± 0.17	1.83	1.91
1ES 0347−121	0.188	Aharonian et al. (2007a)	HESS	0.25	3.0	$3.10 \pm 0.23 \pm 0.10$	1.94	2.03
1ES 1011+496 (+)	0.212	Albert et al. (2007d)	MAGIC	0.12	0.75	4.00 ± 0.50	2.95	3.10
S5 0716+714 (+)	0.31[a]	Mazin et al. (2009)	MAGIC	0.2	0.7	3.45 ± 0.54	1.47	1.74
PKS 1222+21 (+)	0.432	Aleksić et al. (2011a)	MAGIC	0.07	0.4	$3.75 \pm 0.27 \pm 0.2$	2.32	2.60
3C 66A (+)	0.44[a]	Acciari et al. (2009b)	VERITAS	0.2	0.5	$4.1 \pm 0.4 \pm 0.6$	1.34	1.75
3C 279 (+)	0.536	Albert et al. (2008)	MAGIC	0.09	0.48	4.11 ± 0.68	2.71	2.14
3C 279 (+)	0.536	Aleksić et al. (2011b)	MAGIC	0.15	0.35	3.1 ± 1.1	0.51	0.97

[a]The redshifts of 3C 66A and S5 0716+714 quoted here are considered uncertain; see references for details.

most simple theoretical form of the spectra from SSC emission is a double-peaked distribution (when plotted as νF_ν), which arises from synchrotron radiation of lower energy photons and inverse Compton upscattering of those same photons to gamma-rays. In this model, the power law measured at VHE scales is an approximation to a section of the inverse Compton peak.

Furthermore, the effect of gamma-ray attenuation through pair production does not in general preserve a power-law form, as can be seen in the optical depth plot, Fig. 7. Quantifying attenuation as a simple modification to an intrinsic spectral index is an approximation that is only valid when considering short intervals in energy and fairly low redshifts. The EBL attenuation has also been described as a decaying exponential function in energy that affects the spectra above some threshold. However, this is a misleading functional description of the optical depth. The sharp increase in absorption in Fig. 7 that appears at multi-TeV energies is caused by the rapid increase in photon density as one transitions from the mid-IR minimum in the EBL SED and into the redshift-broadened PAH region and far-IR peak (note that our SED is plotted in terms of flux density, not number density). This part of the EBL is created by re-emitted light from cold dust, much of which originates in rapidly star-forming galaxies, and there is no reason to believe that this absorption feature would be related to an exponential form. The power law and the exponential cut-off, which are often used to describe gamma-ray spectra, are not amenable to describing the full non-linear effects of EBL absorption, which is a line-of-sight integral over the evolving photon field. Our optical depths for nearby sources are relatively straight from a couple hundred GeV out to this turnover region, so we present results for sources with spectra measured in this energy range.

One other note concerns the integration over bins of finite width in energy. As attenuation differs across these intervals, it changes the weighting of data and therefore the mean within the bin. Properly de-absorbing spectral data points requires incorporating the optical depth into the analysis used to produce the points, and not just multiplying by e^τ at the mean of the bin. Correlations between the data points must also be accounted for in effectively measuring error. The effect of scaling the data with a simple multiplication introduces error that is likely to grow with redshift.

Having warned the reader of these caveats, we present results for known blazars seen above ∼100 GeV in Table 2. The results in the table are also shown in graphical form in Fig. 10. This plot shows the amount of change in spectral index after EBL deconvolution for a number of blazars, as a function of source redshift. The majority of the objects presented here are of the high frequency-peaked BL Lac (HBL) type, with the exceptions of intermediate-peaked W Comae and 3C 66A, low-peaked BL Lacertae and S5 0716+714, and flat spectrum radio quasars 3C 279 and PKS 1222+21.

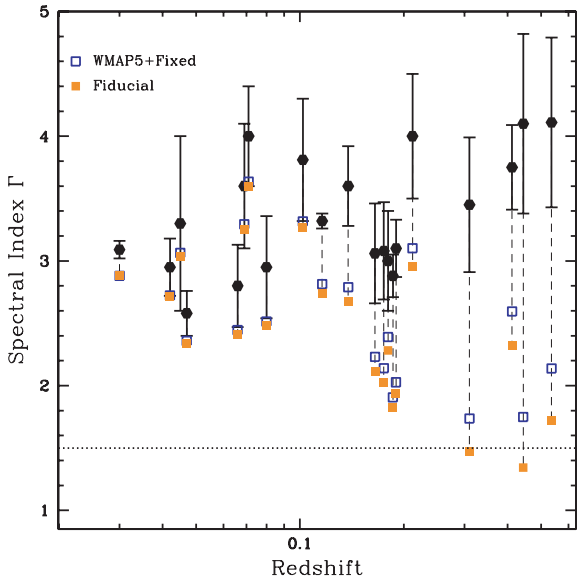

Figure 10. Here we show the results of Table 2 in graphical form. The measured spectral index (Γ; $dN/dE \propto E^{-\Gamma}$) and redshift of each blazar is shown as a black hexagon with error bars, with the index corrected via the fiducial EBL shown as a solid orange point, and that corrected by the *WMAP*5+fixed model as an open blue point. The horizontal dotted line shows $\Gamma = 1.5$, which is typically taken as the hardest spectrum possible under usual assumptions. Some points have been shifted sideways slightly for readability.

Values from this table should only be taken as approximate, particularly for more distant sources. To avoid the hazards of analysing data bin-by-bin, as mentioned in the previous paragraph, we have based our results here on the spectral indices and applicable energy ranges as derived by the authors referenced, whenever possible. In the cases where the spectrum is claimed to continue above the turnover in optical depths seen at several TeV, the results become strongly dependent upon the highest energy extent of the fit. When an explicit value is not mentioned, we use the highest energy point displayed in the spectrum in the reference. It is argued in at least a couple of cases (Mrk 421 and 501; Konopelko et al. 2003) that the de-absorbed spectrum shows the rollover at the top of the IC peak. Recent MAGIC observations of Mrk 501 have detected a spectral peak at energies which vary in correlation with flaring activity (Albert et al. 2007e). As simple power-law functions do not provide a good fit in this case, we have omitted Mrk 501 from our analysis.

Two spectra in our analysis show unusually hard reconstructed spectra. In the case of H1426+428 (Aharonian et al. 2002), the reported spectrum that we have used does not conform well to a power law, a fact that the authors attribute to EBL absorption, and to be cautious we have used an upper energy of 6 TeV. The spectral index of 1ES 0229+200 (Aharonian et al. 2007b) is sensitive to the highest energies used in the calculation, and we assume here an upper energy of 7 TeV, which is close to the second-highest data point presented in the reference. In general, the reconstructed spectral indices for spectra extending above a few TeV are highly sensitive to the highest energy data point considered due to the rapid increase in opacity with energies at this scale (Fig. 7).

It is also interesting to compare the effect that dust modelling has on spectral reconstruction, by comparing the results of the fixed and evolving (fiducial) treatments in the *WMAP*5 model. The former produces an EBL that is slightly more intense in the mid-IR, while at shorter wavelengths the evolving dust treatment of the fiducial model allows a higher optical and near-IR intensity. Higher redshift blazars have generally only been seen at lower energies, where gamma-ray attenuation is produced by the optical–near-IR EBL peak created mostly by redshifted direct starlight. As can be seen in Table 2 and Fig. 10, the larger optical and near-IR flux of the fiducial model produces more spectral change than the fixed model in most blazars. For a few blazars that have been seen to multi-TeV energies, the fixed model produces a harder slope.

As mentioned in Acciari et al. (2009b), determining the redshift of blazars can be difficult due to the lack of strong line emission. Blazars S5 0716+714, PG 1553+113 and 3C 66A are cases where VHE spectra have been published, but the source redshift remains uncertain. With a given background model, gamma-ray attenuation can be used to place upper redshift limits on these sources (e.g. Prandini et al. 2010; Yang & Wang 2010). Applying the standard $\Gamma \geq 1.5$ constraint, we have summarized some findings for these redshift constraints in Table 3. Here, we use the upper 1σ bound on source spectral index as the basis for the limit. The redshift of 3C 66A was initially determined to be 0.444 from a single emission line, taken to be magnesium-II, and corroborated by a weak Lyα detection. Assuming this is correct, we find for this blazar a reconstructed spectrum that is harder than many others on the list, but still significantly softer than the standard limit at the 1σ uncertainty bound. The HBL PG 1553+113 has been detected by both MAGIC (Albert et al. 2007a) and HESS (Aharonian et al. 2008a), but the redshift remains unknown at this time. Observations with the HST have been unable to find a precise distance, but suggest a redshift in the range $0.3 < z < 0.4$ (Treves, Falomo & Uslenghi 2007), potentially making this the most distant VHE-detected HBL. Studies of the intervening Lyα forest with Cosmic Origins Spectrograph (COS; Danforth et al. 2010) have more recently found a higher redshift bound, $z > 0.395$. Our most stringent constraints with the *WMAP*5 model put this blazar at $z < 0.40$ with the spectral index presented by Prandini et al. (2009), or $z < 0.48$ if the index is taken at the upper 1σ level. A similar analysis by Mazin

Table 3. Here we show the upper redshift limits for three blazars with uncertain redshift based on the $\Gamma \geq 1.5$ criterion discussed in the last section, and using the upper 1σ uncertainty bound on the spectral indices. Some of these blazars were also shown in Table 2, assuming there the most likely source redshift.

Object ID	Reference	Experiment	$E_{L\gamma}$	$E_{H\gamma}$	$\Gamma_{\rm obs}$	z fiducial	z fixed
S5 0716+714 (+)	Mazin et al. (2009)	MAGIC	0.2	0.7	3.45 ± 0.54	<0.37	<0.42
PG 1553+113 (+)	Wagner et al. (2008)	MAGIC	0.09	0.5	4.2 ± 0.3	<0.62	<0.72
PG 1553+113	Prandini et al. (2009)	MAGIC	0.15	0.6	4.12 ± 0.17	<0.48	<0.51
PG 1553+113	Aharonian et al. (2008a)	HESS	0.23	1.3	4.5 ± 0.32	<0.48	<0.52
3C 66A (+)	Acciari et al. (2009b)	VERITAS	0.2	0.5	$4.1 \pm 0.4 \pm 0.6$	<0.53	<0.56

& Goebel (2007) using MAGIC data and a low-level EBL similar to the level set by galaxy counts found $z < 0.69$, while Prandini et al. (2009) placed a limit $z < 0.67$ with the model of Kneiske & Dole (2010). This blazar was also considered in D11, and an upper redshift of $z \leq 0.85 \pm 0.07$ was found. Reconstructing the intrinsic spectrum at higher redshifts also was found to lead to a break in the power-law shape. Demanding that such a break be absent leads to a tighter upper limit in this reference, $z < 0.42$. The weight of this evidence would seem to suggest a redshift near the lower limit set by Danforth. S5 0716+714 is an LBL for which a spectrum has been recently reported by MAGIC, and was previously detected by EGRET and AGILE. Our fiducial bound of $z < 0.31$ ($z < 0.37$ at 1σ) is in agreement with the range reported by Nilsson et al. (2008), $z = 0.31 \pm 0.08$.

4 COMPARISON WITH OTHER WORK

In this section we compare the methodology and results of our EBL determination with others in the recent literature, including the previous predictions of earlier versions of our SAM. Our prior prediction for the EBL, presented in Primack et al. (2005), used a similar SAM of structure formation to that which we have used in this work and in Primack et al. (2008). The *WMAP*5 model presented here has similar normalization to the 2005 model in the optical and near-IR, leading to low flux in these wavebands, with only a small amount of light unresolved in the deepest number count surveys. The differences in the spectral shape of the optical peaks are due to changes in the application of the dust absorption prescriptions; in this work and in Primack et al. (2008) we use the two-component model of Charlot & Fall (2000), which leads to more absorption in the UV and emission in the mid- and far-IR. A comparison of the different emission templates was presented in SGPD12. The CΛCDM model we have presented features a higher level of star formation, particularly at early times, as a result of assuming a larger normalization in the initial dark matter power spectrum. In the mid- and far-IR, all of our new models produce significantly more light due to a larger energy budget from absorbed starlight. While the prior prediction was not able to match the level of light suggested by the number counts with ISOCAM at 15 μm or the level of far-IR flux inferred from DIRBE and FIRAS, all of our new models are consistent with constraints from number counts in the mid- and far-infrared and with FIRAS, and are near the lower determinations of the DIRBE instrument at 140 and 240 μm. The *AKARI* measurements of Matsuura et al. (2011) and some DIRBE measurements (Schlegel et al. 1998) do suggest a larger flux in the far-IR peak.

The EBL model of Franceschini et al. (2008) is based on luminosity functions from a variety of survey data. Recognizing the need for separate treatments of evolution in different wavelength regimes, this model treats optical and IR components separately, using the recent body of data from *Spitzer* and other experiments. Near-IR luminosity function data up to $z = 1.4$ is used for the spiral and spheroidal populations, while only local luminosity functions are used for the irregular population. Other local IR data are used to constrain other regions of the spectrum. The EBL model presented by these authors is similar to ours at most wavelengths except the far-IR peak. As their model has been derived from the same body of cosmological data that our own has been compared against, it is not surprising to see similar predictions at low redshift. In Fig. 11 we show the EBL evolution and gamma-ray attenuation predictions from our models compared with those of Franceschini et al. (2008), as well as D11, model 'C' in Finke et al. (2010), both predictions of Stecker et al. (2006) and the best-fitting model in Kneiske et al. (2004), which we will discuss in the following paragraphs. Our model is seen to evolve similarly to the Franceschini model out to redshift 1.

The work of Kneiske et al. (2002) calculated the EBL from the UV to far-IR using a 'semi-empirical' method based on measured SFRs and spectral synthesis models. Starlight is processed by dust, which is modelled as a blackbody with three temperature components.

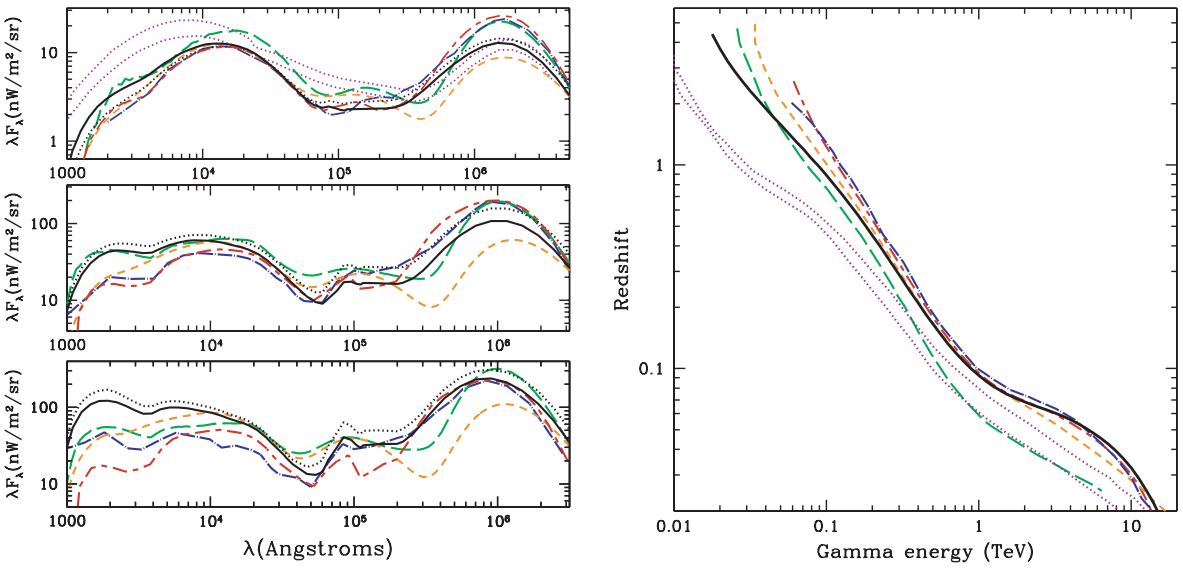

Figure 11. Left: our EBL predictions compared with several recent models from the literature. Solid and dotted black lines show the proper flux density from our *WMAP*5 and CΛCDM models in the local universe and at $z = 1$ and 2. Other lines are from Franceschini et al. (2008) (dashed–dotted blue), the best-fitting model of (Kneiske et al. 2004) (long-dashed green), D11 (long-short dashed red) and model 'C' from Finke et al. (2010) (dashed orange). The baseline and fast evolution models of Stecker et al. (2006) are the low and high dotted violet points in the $z = 0$ panel. Right: a comparison of the $\tau_{\gamma\gamma} = 1$ attenuation edges for several models. Line types are as in the opposite panel. In this instance, the lower set of dotted points denotes the fast evolution model of Stecker et al. (2006), while the upper are the baseline model.

Metallicity is assumed to increase slowly over cosmic time and an average global extinction curve applied to starlight. A follow-up paper, Kneiske et al. (2004), expanded this earlier model into six realizations, varying in gas temperature contribution, SFR and UV escape fraction. The 'best-fitting' EBL in this paper is considerably higher than any of our models in both the optical and far-IR peaks. The discrepancy in EBL normalization between this model and our own likely originates in the SFR densities assumed, which have a much different functional form than our model. Knieske's results are based upon a broken power law for the star formation history, with a peak at $z = 1.2$. The history predicted by our model is considerably lower in this epoch, and does not peak until $z \approx 3$ for our ΛCDM model, or $z \approx 2.5$ for the *WMAP*5 model (Fig. 1). Thus our models have a lower present-day flux, but higher flux at the location of Kneiske's peak and at higher redshifts. The use of a blackbody spectrum to approximate emission in the PAH region also gives their EBL SED a somewhat different shape in the mid-IR than we find with our templates which include these sharp emission features. The update to this model in Kneiske & Dole (2010) produces a background flux that is close to the level seen in discrete number counts from the optical to mid-IR, and is similar to our fiducial model.

The recent models presented in Finke et al. (2010) are based on a similar technique to Kneiske's work. These models are built from the earlier models in Razzaque et al. (2009), in which the contribution to the EBL from main-sequence stars was found by computing stellar emissivities after assuming forms for the global star formation history and IMF. Finke et al. (2010) expanded these models by including dust re-absorption and emission, as well as post-main-sequence stars. The authors favour their model ('C') with a Baldry & Glazebrook (2003) IMF and star formation history from Hopkins & Beacom (2006) with Cole et al. (2001) parametrization. The Baldry–Glazebrook IMF produces slightly more high-mass stars than the Chabrier IMF that we have used. This model has a slightly higher normalization than ours in the optical and near-IR. In the mid- and far-IR, we find considerably different SED shapes due to the use of different techniques in modelling dust emission, as was the case with the models of Kneiske et al.; we have used templates which are based on the galaxies' total IR emission, while these models assume thermal blackbody emission at three fixed temperatures.

The models of Stecker and collaborators, most recently Stecker et al. (2006, 2007), have explored the background using backward evolution models. This most recent work proposed two SEDs for the EBL, using two different assumptions about the pure luminosity evolution of the 60 μm luminosity function. The SEDs of all galaxies are assumed to be determined by this 60 μm emissivity. The 'baseline' model features a pure luminosity evolution multiplier of $(1+z)^{3.1}$ out to $z = 1.4$, and constant luminosity from there to $z = 6$. The 'fast evolution' model evolves even more quickly, as $\sim(1+z)^4$ to $z = 0.8$ and $\sim(1+z)^2$ for $0.8 < z < 1.5$. Both of these models are considerably higher than ours in the optical and near-IR, with the fast evolution model about 50 per cent higher in this range than the baseline; the discrepancy in the far-IR with our models is smaller. It is difficult to compare our model, which deals with galaxies in a system of hierarchically merging dark matter haloes, with this model, in which it is assumed that the local galaxy population just grows brighter with increasing redshift. Our 60 μm luminosity density is not found to increase nearly as quickly as assumed in either of these models; we find that both of our models can be well described by a luminosity density multiplier of $\sim(1+z)^{1.7}$ out to $z \approx 1.4$ at this wavelength. As mentioned in the Introduction, the high optical and near-IR flux of the fast-evolution model puts it at odds with the detection of 3C 279 by MAGIC (Albert et al. 2008), which was disputed by Stecker in another analysis (Stecker & Scully 2009). However, the large error on the determined de-absorbed spectral index (0.5 ± 1.2), and the possibility of hardening of the spectrum by internal absorption (Aharonian, Khangulyan & Costamante 2008c; Liu, Bai & Ma 2008, but see also Tavecchio & Mazin 2009), make it difficult to claim this observation as a firm limit on the EBL. Further observations of this and other high-redshift sources will likely improve constraints on flux in the optical EBL peak. As mentioned above, both models in this work are in serious conflict with the limits set by high-redshift blazars observed by *Fermi* LAT (Abdo et al. 2010b).

A comparison of the model of D11 with our fiducial model has been presented and discussed in that work. Overall, we find good agreement with D11 from optical to mid-IR wavelengths from the local universe to $z = 1$. At longer wavelengths, D11 predicts considerably more flux from starlight reprocessed by cold dust in galaxies. The large discrepancy in results for the far-IR peak in the EBL highlights the uncertainties involved in modelling this region, an ongoing challenge which we address at the end of the next section. Discrepancies in this region only have an observable effect on the gamma-ray spectra for the closest blazars. The SFR implied in D11 (see fig. 12 in that work) is considerably higher than our own, and increases more rapidly with redshift between $z = 0$ and 1. At UV wavelengths, our model produces more light than predicted in D11, and more absorption of gamma-rays below ∼300 GeV. As shown in SGPD12, the UV luminosity in our model is near the largest values measured across redshift in integrated luminosity functions, and can be considered a maximal prediction at these short wavelengths.

At nearly all wavelengths we have considered, our fiducial EBL SED is near the level of flux resolved in discrete background counts, and we find agreement with the claim of Madau & Pozzetti (2000) that nearly all light in the optical EBL peak is produced by discrete sources. Referring back to Fig. 4, we recognize two places in our calculated EBL SED in which there is tension with observations that do not rely strongly on foreground estimates, and which may signal shortcomings in our spectral modelling. In the UV, we find an EBL lower than calculated using a combination of HDF and balloon-based FOCA data (Gardner et al. 2000). The later *GALEX* experiment, while not capable of surveying to the depth of Hubble, found a smaller number of bright counts than the FOCA data, likely resulting from differences in calibration of the instruments (Xu et al. 2005). It is therefore possible that the higher Gardner points resulted from overestimating the bright counts in their determination. Our prediction for the local EBL is above the integrated number count measurements of Grazian et al. (2009) in the *U* band and Dolch & Ferguson (in preparation) in the *F435W* band; in the former there is significant disagreement with Madau & Pozzetti (2000) at faint magnitudes, but confirmation that the counts are convergent. In the near-IR, we find good agreement with published results from Madau & Pozzetti (2000) and Keenan et al. (2010). Our models fall about 1σ below the 5.6 μm lower bound from *Spitzer*. The fact that the 5.6 μm limit is higher than that at 4.5 may cast some suspicion on this particular measurement, as there is no reason to believe such a spectral feature would exist. These lower limits are based upon early 'first-look' data, and newer results based on a larger set of survey data should soon be available (G. Fazio, private communication). Additional sensitivity and survey width may be achievable in the 3.6 and 4.5 μm bands by post-cryogenic 'Warm *Spitzer*' surveys; however, the longer wavelength bands

will not be attainable at elevated temperatures (van Dokkum et al. 2007).

Our models lie below the level of direct detection of the absolute background by calculations using data from Hubble Wide Field and Planetary Camera 2 (WFPC2), DIRBE and *IRTS* (see the discussion for Fig. 4), however, we do find consistency with the newer optical results of Mattila et al. (2011), and also the Pioneer analysis of Matsuoka et al. (2011). The low significance and large error bars on the *HST* points of Bernstein (2007) mean that these results should not be considered inconsistent with an EBL at the level provided by resolved sources. All of our models are at least 1σ below the flux from any of the near-IR direct detection calculations we have discussed. Limits from gamma-ray observations shown in Fig. 9 have strongly disfavoured the highest levels at this range. As discussed in Levenson et al. (2007), the present uncertainty in zodiacal light subtraction may be intractable without a new mission to directly study this foreground, such as the proposed ZEBRA experiment (see discussion in Zemcov et al. 2011). While our models are consistent within 1σ with number count measurements by MIPS in the mid- and far-IR, they are low compared to the DIRBE measurements of the far-IR peak. The zodiacal foreground is a sharply decreasing function of wavelength in this regime, and the DIRBE points are expected to suffer from less systematic error here than in the near-IR, especially at 240 μm, where our models lies beneath the data. However, our IR templates include a somewhat simplified treatment of blackbody emission at these long wavelengths, and we do not expect accurate reproduction in this regime.

Fardal et al. (2007) compared the possible range of EBL flux measurements with observations of the fossil mass and SFR history of the universe. As our SAM reproduces these three observables, it is worth discussing our work in the context of their claim that a top-heavy or 'paunchy' IMF can best fit simultaneously these data. This proposal is based on the argument that the low levels of estimated stellar mass are difficult to reconcile with the present-day EBL flux suggested as being intermediate between the direct detections and the lower limits from resolved galaxies, which is now known to be in conflict with blazar limits (see Fig. 9). Fardal et al. (2007) created three models of the EBL based on all available observational limits. Their minimal model, with total flux of $50\,\mathrm{nW\,m^{-2}\,sr^{-1}}$, is set by resolved number counts and is similar to our *WMAP*5 and CΛCDM models in the optical and near-IR out to the *K* band. Their best-fitting model, based on a compromise between number counts compilations and the *HST* and DIRBE direct detection measurements, is substantially higher than our CΛCDM model. The *K*-band number counts are well measured by a number of surveys (see fig. 14 in SGPD12) which constrain the amount of stellar mass in the nearby universe. Two factors alleviate the discrepancy in our model. Our background fluxes are near the lowest levels considered in Fardal et al. (2007), with total fluxes of 56.09 and $54.91\,\mathrm{nW\,m^{-2}\,sr^{-1}}$ for our CΛCDM and *WMAP*5 models, respectively (Table 1), and our global Chabrier IMF produces more high-mass stars than the diet-Salpeter considered as the standard by these authors. For a near-IR flux much higher than our models to not overproduce the *K*-band counts, this flux would have to arise from a high-redshift population of sources unresolvable in our current surveys, which extend to >24 mag. As mentioned in the Introduction, there are reasons why the SFR measures we compare against at high redshift could be biased high. This interpretation favours our fiducial EBL model, which has slightly less flux than Fardal's lowest model, and is in fairly good agreement with integrated star formation and observed *K* counts (see SGPD12).

5 DISCUSSION

The EBL presents one of the primary barriers to extragalactic gamma-ray astronomy with ground-based instruments. Our determination of a fairly low extragalactic background across the optical and near- to mid-IR, supported by convergence with alternative methods such as Franceschini et al. (2008) and D11 as well as new direct measurement techniques and recent limits from gamma-ray experiments in the optical to mid-IR, is an optimistic prediction for the future of the field. The weight of this evidence also increasingly points to an EBL that is well known over this wavelength range, at a level near that of resolved number counts, though many questions remain about its redshift evolution. The ability of current- and next-generation experiments to detect blazars at larger distances is a function of several factors: the luminosity function and spectral evolution of these objects, the effective area (especially at the lowest energies) and duty cycles of these instruments, and the details of the increasingly uncertain non-local EBL at higher redshifts. The field of extragalactic VHE astronomy has grown considerably in the last 5 yr, and ongoing progress on the instrumentation front suggests that many new detections may be coming. In Fig. 8, we have placed vertical lines at 50 and 100 GeV to facilitate comparison with the gamma-ray attenuation edge curves. In the fiducial *WMAP*5 model, the universe does not become optically thick ($\tau > 1$) to 100 GeV gamma-rays until $z \sim 0.9$, and $z \sim 1.6$ for an observed energy of 50 GeV. Our fiducial model does predict slightly higher opacities at high redshift compared to the fiducial model of Gilmore et al. (2009); this is due to more UV light escaping high-redshift galaxies in our evolving dust model than in the fixed dust model used in the CΛCDM prediction. Nonetheless, the EBL does not become a significant barrier to VHE observations at these low energies in either model until redshifts considerably higher than those for which AGN have presently been detected by ground-based instruments. At the redshift of the current most distant confirmed source, 3C 279, we find $\tau = 0.38$ for an observed energy of 100 GeV, and $\tau = 1$ at 175 GeV.

As mentioned, the approximation of a local EBL in optical depth calculations is only valid for nearby extragalactic observations. At redshifts above ∼0.3, differences in the evolution of star formation and galaxy emissivity begin to have a substantial effect on attenuation; two different EBL models with the same present-day normalization could have widely varying behaviour at these times. For instance, the Kneiske models and Stecker's fast evolution models have star formation history peaks at a lower redshift than our models predict. In addition to predicting different results for the present-day EBL than our model, the evolution with redshift is also quite a bit different in these cases. As no direct observations of the EBL are possible at non-zero redshift, predicting attenuation from sources past these distances must be made on the basis of models of galaxy evolution, constrained by surveys of luminosity functions at high redshift. Recent surveys of the non-local universe such as DEEP2 and the multiwavelength GOODS and AEGIS surveys have become powerful tools in constraining the EBL at these distances. Observational methods such as Franceschini et al. (2008), Finke et al. (2010) and D11, which fall under types (ii), (iii) and (iv), respectively, in the classification scheme discussed in the Introduction, are complementary to our semi-analytic approach, which is of the first type. Beyond $z \sim 1$ to 2, uncertainties in available star formation and luminosity data become large, and theoretical models will continue to be required to understand the production and evolution of the background.

The other impact of the shift to higher redshift observations by lower energy-threshold instruments such as the HESS phase-II upgrade and the future Cherenkov Telescope Array (CTA) experiment is the change in the relevant absorbing photon population to UV wavelengths. Our models, and the others we reference in the previous section, predict a rapid falloff in transmission of gamma-rays above 500 GeV for blazars at the redshift of 3C 279. Detecting emission at or above 1 TeV from sources at this distance will require orders-of-magnitude gains in instrument effective area, or observations of flare events with similar increases in output. The energy range of primary interest for these types of sources is going to be 50 to 500 GeV for the next generation of IACTs, plus lower energy data from *Fermi*. Below 200 GeV, it is the UV background that is primarily responsible for absorption. In Gilmore et al. (2009), we addressed the question of this background using four different models varying in high redshift star formation and quasar emissivity; the 'fiducial' model in that paper that we consider to be the most likely was based on the CΛCDM model in this work. The *WMAP*5 model with evolving dust parameters presented in this work is generally consistent with this model in its predictions for the evolution of UV emission, though it does predict a somewhat stronger UV background at high redshift.

One significant weakness of our present approach is our use of templates to describe re-emission by dust at mid- and far-IR wavelengths, which is relevant to the interpretation of multi-TeV data from nearby blazars. This method makes the assumption that galaxies of a given bolometric luminosity emit light with a similar spectral distribution. As discussed in SGPD12, future progress in understanding these wavelengths will likely require moving past this assumption. While there is much progress to be made modelling this part of the background SED, new models of dust will only have a substantial effect on our calculation of gamma-ray opacities for the nearest VHE sources.

ACKNOWLEDGMENTS

AD, RCG and JRP acknowledge support from a *Fermi* Guest Investigator Grant. RCG and JRP were also supported by NASA ATP grant NNX07AGG4G, NSF-AST-1010033 and NSF-AST-0607712. RCG was supported during this work by a SISSA postdoctoral fellowship. RSS and RCG thank UCSC for hospitality during many visits. AD's work has been supported by the Spanish Ministerio de Educación y Ciencia and the European regional development fund (FEDER) under projects FIS2008-04189 and CPAN-Ingenio (CSD2007-00042), and by the Junta de Andalucía (P07-FQM-02894).

We wish to thank Felix Aharonian, David A. Williams, Amy Furniss and A. Nepomuk Otte for helpful discussions concerning gamma–ray attenuation. Fabio Fontanot assisted in comparisons of different dust templates.

The TeVCat (http://tevcat.uchicago.edu/) online TeV-source catalogue was used in the preparation of this paper.

REFERENCES

Abdo A. A. et al., 2010a, ApJ, 715, 429
Abdo A. A. et al., 2010b, ApJ, 723, 1082
Acciari V. et al., 2009a, ApJ, 690, L126
Acciari V. A. et al., 2009b, ApJ, 693, L104
Aharonian F. A., 2001, in Gladysheva O. G., Kocharov G. E., Kovaltsov G. A., Usoskin I. G., eds, Int. Cosmic Ray Conf. Vol. 27, 27th International Cosmic Ray Conference, Hamburg, Germany, 07-15th August 2001. Copernicus Gesellschaft, Berlin, p. 250
Aharonian F. A. et al., 1999, A&A, 350, 757
Aharonian F. et al., 2002, A&A, 384, L23
Aharonian F. et al., 2005a, A&A, 430, 865
Aharonian F. et al., 2005b, A&A, 436, L17
Aharonian F. et al., 2006, Nat, 440, 1018
Aharonian F. et al., 2007a, A&A, 473, L25
Aharonian F. et al., 2007b, A&A, 475, L9
Aharonian F. et al., 2008a, A&A, 477, 481
Aharonian F. et al., 2008b, A&A, 481, L103
Aharonian F. A., Khangulyan D., Costamante L., 2008c, MNRAS, 387, 1206
Albert J. et al., 2006a, ApJ, 639, 761
Albert J. et al., 2006b, ApJ, 642, L119
Albert J. et al., 2006c, ApJ, 648, L105
Albert J. et al., 2007a, ApJ, 654, L119
Albert J. et al., 2007b, ApJ, 662, 892
Albert J. et al., 2007c, ApJ, 666, L17
Albert J. et al., 2007d, ApJ, 667, L21
Albert J. et al., 2007e, ApJ, 669, 862
Albert J. et al., 2008, Sci, 320, 1752
Aleksić J. et al., 2011a, ApJ, 730, L8
Aleksić J. et al., 2011b, A&A, 530, 4
Arnouts S. et al., 2007, A&A, 476, 137
Atwood W. B. et al., 2009, ApJ, 697, 1071
Baldry I. K., Glazebrook K., 2003, ApJ, 593, 258
Barro G. et al., 2009, A&A, 494, 63
Bell E. F., McIntosh D. H., Katz N., Weinberg M. D., 2003, ApJS, 149, 289
Bernstein R. A., 2007, ApJ, 666, 663
Berta S. et al., 2010, A&A, 518, L30
Béthermin M., Dole H., Beelen A., Aussel H., 2010, A&A, 512, A78
Blanton M. R. et al., 2003, ApJ, 592, 819
Bouwens R. J., Illingworth G. D., Franx M., Ford H., 2007, ApJ, 670, 928
Bruzual G., Charlot S., 2003, MNRAS, 344, 1000
Calzetti D., Armus L., Bohlin R. C., Kinney A. L., Koornneef J., Storchi-Bergmann T., 2000, ApJ, 533, 682
Cambrésy L., Reach W. T., Beichman C. A., Jarrett T. H., 2001, ApJ, 555, 563
Caputi K. I. et al., 2007, ApJ, 660, 97
Chabrier G., 2003, PASP, 115, 763
Charlot S., Fall S. M., 2000, ApJ, 539, 718
Chary R. et al., 2004, ApJS, 154, 80
Cogan P., 2008, in Aharonian F. A., Hofmann W., Rieger F., eds, AIP Conf. Ser. Vol. 1085, 4th International Meeting on High Energy Gamma-Ray Astronomy Am. Inst. Phys., New York, p. 403
Cole S. et al., 2001, MNRAS, 326, 255
Cortina J., 2005, Ap&SS, 297, 245
da Cunha E., Charlot S., Elbaz D., 2008, MNRAS, 388, 1595
Dahlen T., Mobasher B., Somerville R. S., Moustakas L. A., Dickinson M., Ferguson H. C., Giavalisco M., 2005, ApJ, 631, 126
Dahlen T., Mobasher B., Dickinson M., Ferguson H. C., Giavalisco M., Kretchmer C., Ravindranath S., 2007, ApJ, 654, 172
Danforth C. W., Keeney B. A., Stocke J. T., Shull J. M., Yao Y., 2010, ApJ, 720, 976
Daniel M. K. et al., 2005, ApJ, 621, 181
Devlin M. J. et al., 2009, Nat, 458, 737
Devriendt J. E. G., Guiderdoni B., 2000, A&A, 363, 851
Devriendt J. E. G., Guiderdoni B., Sadat R., 1999, A&A, 350, 381
Dole H. et al., 2006, A&A, 451, 417
Domínguez A. et al., 2011, MNRAS, 410, 2556 (D11)
Dwek E., Krennrich F., 2005, ApJ, 618, 657
Faber S. M. et al., 2007, ApJ, 665, 265
Fardal M. A., Katz N., Weinberg D. H., Davé R., 2007, MNRAS, 379, 985
Fazio G. G. et al., 2004, ApJS, 154, 39
Finke J. D., Razzaque S., Dermer C. D., 2010, ApJ, 712, 238
Fixsen D. J., Dwek E., Mather J. C., Bennett C. L., Shafer R. A., 1998, ApJ, 508, 123

Fortin P., 2008, in Aharonian F. A., Hofmann W., Rieger F., eds, AIP Conf. Ser. Vol. 1085, 4th International Meeting on High Energy Gamma-Ray Astronomy Am. Inst. Phys., New York, p. 565
Franceschini A., 2001, in Harwit M., Hauser M. G., eds, Proc. IAU Symp. 204, The Extragalactic Infrared Background and Its Cosmological Implications. Astron. Soc. Pac., San Francisco, p. 283
Franceschini A., Aussel H., Cesarsky C. J., Elbaz D., Fadda D., 2001, A&A, 378, 1
Franceschini A., Rodighiero G., Vaccari M., 2008, A&A, 487, 837
Frayer D. T. et al., 2006, ApJ, 647, L9
Gabasch A. et al., 2006, A&A, 448, 101
Gardner J. P., Brown T. M., Ferguson H. C., 2000, ApJ, 542, L79
Gilmore R. C., Madau P., Primack J. R., Somerville R. S., Haardt F., 2009, MNRAS, 399, 1694
Gorjian V., Wright E. L., Chary R. R., 2000, ApJ, 536, 550
Gould R. J., Schreder G. P., 1967, Phys. Rev., 155, 1404
Grazian A. et al., 2009, A&A, 505, 1041
Hauser M. G., Dwek E., 2001, ARA&A, 39, 249
Hinton J. A., 2004, New Astron. Rev., 48, 331
Hopkins A. M., Beacom J. F., 2006, ApJ, 651, 142
Hopwood R. et al., 2010, ApJ, 716, L45
Jauzac M. et al., 2011, A&A, 525, A52
Jelley J. V., 1966, Phys. Rev. Lett., 16, 479
Jones D. H., Peterson B. A., Colless M., Saunders W., 2006, MNRAS, 369, 25
Katarzyński K., Ghisellini G., Tavecchio F., Gracia J., Maraschi L., 2006, MNRAS, 368, L52
Keenan R. C., Barger A. J., Cowie L. L., Wang W., 2010, ApJ, 723, 40
Kennicutt R. C., Jr, 1989, ApJ, 344, 685
Kennicutt R. C., Jr, et al., 1998, ApJ, 498, 181
Kneiske T. M., Dole H., 2010, A&A, 515, A19
Kneiske T. M., Mannheim K., Hartmann D. H., 2002, A&A, 386, 1
Kneiske T. M., Bretz T., Mannheim K., Hartmann D. H., 2004, A&A, 413, 807
Kochanek C. S. et al., 2001, ApJ, 560, 566
Komatsu E. et al., 2011, ApJS, 192, 18
Konopelko A., Mastichiadis A., Kirk J., de Jager O. C., Stecker F. W., 2003, ApJ, 597, 851
Konopelko A., Cui W., Duke C., Finley J. P., 2008, ApJ, 679, L13
Lagache G., Puget J.-L., Dole H., 2005, ARA&A, 43, 727
Le Floc'h E. et al., 2005, ApJ, 632, 169
Le Floc'h E. et al., 2009, ApJ, 703, 222
Levenson L. R., Wright E. L., 2008, ApJ, 683, 585
Levenson L. R., Wright E. L., Johnson B. D., 2007, ApJ, 666, 34
Liu H. T., Bai J. M., Ma L., 2008, ApJ, 688, 148
Madau P., Phinney E. S., 1996, ApJ, 456, 124
Madau P., Pozzetti L., 2000, MNRAS, 312, L9
Madau P., Pozzetti L., Dickinson M., 1998, ApJ, 498, 106
Maier G. et al., 2008, in Caballero R., D'Olivo J. C., Medina-Tanco G., Nellen L., Sánchez F. A., Valdés-Galicia J. F., eds, Int. Cosmic Ray Conf. Vol. 3, 30th International Cosmic Ray Conference, ICRC, p. 1457. Available online at http://www.icrc2007.unam.mx/proceedings
Malkan M. A., Stecker F. W., 1998, ApJ, 496, 13
Malkan M. A., Stecker F. W., 2001, ApJ, 555, 641
Marchesini D. et al., 2007, ApJ, 656, 42
Matsumoto T. et al., 2005, ApJ, 626, 31
Matsuoka Y., Ienaka N., Kawara K., Oyabu S., 2011, ApJ, 736, 119
Matsuura S. et al., 2011, ApJ, 737, 2
Mattila K., Lehtinen K., Vaisanen P., von Appen-Schnur G., Leinert C., 2011, preprint (arXiv:1111.6747)
Mazin D., Goebel F., 2007, ApJ, 655, L13
Mazin D., Raue M., 2007, A&A, 471, 439
Mazin D., Lindfors E., Berger K., Galante N., Prandini E., Saito T. (for the MAGIC collaboration), 2009, arXiv:0907.0366
Montero-Dorta A. D., Prada F., 2009, MNRAS, 399, 1106
Nikishov A. I., 1962, Soviet Phys. JETP, 14, 393
Nilsson K., Pursimo T., Sillanpää A., Takalo L. O., Lindfors E., 2008, A&A, 487, L29
Oh S. P., 2001, ApJ, 553, 25
Peebles P. J. E., 1993, Principles of Physical Cosmology, Princeton Univ. Press, Princeton, NJ
Pei Y. C., Fall S. M., Hauser M. G., 1999, ApJ, 522, 604
Prandini E., Dorner D., Mankuzhiyil N., Mariotti M., Mazin D. (for the MAGIC Collaboration), 2009, preprint (arXiv:0907.0157)
Prandini E., Bonnoli G., Maraschi L., Mariotti M., Tavecchio F., 2010, MNRAS, 405, L76
Primack J. R., Bullock J. S., Somerville R. S., MacMinn D., 1999, Astropart. Phys., 11, 93
Primack J. R., Somerville R. S., Bullock J. S., Devriendt J. E. G., 2001, in Aharonian F. A., Völk H. J., eds, AIP Conf. Ser. Vol. 558, High Energy Gamma-Ray Astronomy: International Symposium. Am. Inst. Phys., New York, p. 463
Primack J. R., Bullock J. S., Somerville R. S., 2005, in Aharonian F. A., Völk H. J., Horns D., eds, AIP Conf. Ser. Vol. 745, High Energy Gamma-Ray Astronomy. Am. Inst. Phys., New York, p. 23
Primack J. R., Gilmore R. C., Somerville R. S., 2008, in Aharonian F. A., Hofmann W., Rieger F., eds, AIP Conf. Ser. Vol. 1085, 4th International Meeting on High Energy Gamma-Ray Astronomy. Am. Inst. Phys., New York, p. 71
Razzaque S., Dermer C. D., Finke J. D., 2009, ApJ, 697, 483
Reddy N. A., Steidel C. C., Pettini M., Adelberger K. L., Shapley A. E., Erb D. K., Dickinson M., 2008, ApJS, 175, 48
Rieke G. H., Alonso-Herrero A., Weiner B. J., Pérez-González P. G., Blaylock M., Donley J. L., Marcillac D., 2009, ApJ, 692, 556 (R09)
Rodighiero G. et al., 2010, A&A, 515, A8
Rowan-Robinson M., 2001, ApJ, 549, 745
Schiminovich D. et al., 2005, ApJ, 619, L47
Schirber M., Bullock J. S., 2003, ApJ, 584, 110
Schlegel D. J., Finkbeiner D. P., Davis M., 1998, ApJ, 500, 525
Sheth R. K., Tormen G., 1999, MNRAS, 308, 119
Soifer B. T., Neugebauer G., 1991, AJ, 101, 354
Somerville R. S., Primack J. R., 1999, MNRAS, 310, 1087
Somerville R. S., Primack J. R., Faber S. M., 2001, MNRAS, 320, 504
Somerville R. S., Gilmore R. C., Primack J. R., Domínguez A., 2012, MNRAS, doi:10.1111/j.1365-2966.2012.20490 (SGPD12)
Somerville R. S., Hopkins P. F., Cox T. J., Robertson B. E., Hernquist L., 2008, MNRAS, 391, 481 (S08)
Stecker F. W., Scully S. T., 2009, ApJ, 691, L91
Stecker F. W., Malkan M. A., Scully S. T., 2006, ApJ, 648, 774
Stecker F. W., Malkan M. A., Scully S. T., 2007, ApJ, 658, 1392
Superina G. et al., 2008, in Caballero R., D'Olivo J. C., Medina-Tanco G., Nellen L., Sánchez F. A., Valdés-Galicia J. F., eds, Int. Cosmic Ray Conf. Vol. 3, 30th International Cosmic Ray Conference, ICRC, p. 913. Available online at http://www.icrc2007.unam.mx/proceedings
Tagliaferri G. et al., 2008, ApJ, 679, 1029
Takeuchi T. T., Ishii T. T., Hirashita H., Yoshikawa K., Matsuhara H., Kawara K., Okuda H., 2001, PASJ, 53, 37
Tavani M. et al., 2008, Nuclear Instrum. Methods Phys. Res. A, 588, 52
Tavecchio F., Mazin D., 2009, MNRAS, 392, L40
Teshima M. et al., 2008, in Caballero R., D'Olivo J. C., Medina-Tanco G., Nellen L., Sánchez F. A., Valdés-Galicia J. F., eds, Int. Cosmic Ray Conf. Vol. 3, 30th International Cosmic Ray Conference, ICRC, p. 1045. Available online at http://www.icrc2007.unam.mx/proceedings
Toller G. N., 1983, ApJ, 266, 79
Treves A., Falomo R., Uslenghi M., 2007, A&A, 473, L17
van Dokkum P., Cooray A., Labbé I., Papovich C., Stern D., 2007, in Storrie-Lombardi L. J., Silbermann N. A., eds, AIP Conf. Ser. Vol. 943, The Science Opportunities of the Warm Spitzer Mission Workshop. Am. Inst. Phys., New York, p. 122
Wagner R. M., 2008, MNRAS, 385, 119
Wagner R. et al., 2008, in Caballero R., D'Olivo J. C., Medina-Tanco G., Nellen L., Sánchez F. A., Valdés-Galicia J. F., eds, Int. Cosmic Ray Conf. Vol. 3, 30th International Cosmic Ray Conference, ICRC, p. 889. Available online at http://www.icrc2007.unam.mx/proceedings

Wolf C., Meisenheimer K., Rix H.-W., Borch A., Dye S., Kleinheinrich M., 2003, A&A, 401, 73
Wright E. L., 2001, ApJ, 553, 538
Wright E. L., 2004, New Astron. Rev., 48, 465
Wright E. L., Reese E. D., 2000, ApJ, 545, 43
Wyder T. K. et al., 2005, ApJ, 619, L15
Xu C. K. et al., 2005, ApJ, 619, L11
Yang J., Wang J., 2010, A&A, 522, A12
Zemcov M. et al., 2011, preprint (arXiv:1101.1560)

This paper has been typeset from a TEX/LATEX file prepared by the author.